Embedded cluster density approximation for exchange-correlation energy: a natural extension of the local density approximation

Chen Huang*

Department of Scientific Computing and National High Magnetic Field Laboratory, Florida State University, Tallahassee, Florida 32306, USA

E-mail: chuang3@fsu.edu

Abstract

We develop a local correlation method in the framework of Kohn-Sham density functional theory (KS-DFT). The method is termed "embedded cluster density approximation" (ECDA) and is a logical extension of the local density approximation. In ECDA, an embedded cluster is defined for each atom based on the finite-temperature density functional embedding theory. The clusters' XC energy densities are calculated using high-level XC functionals. The system's XC energy is then constructed by patching these locally computed, high-level XC energy densities over the system in an atom-by-atom manner. We derive the relationship between the embedding potential and system's KS potential. We show how to efficiently compute the system's XC potential which is the functional derivative of the patched XC energy with respect to the system's electron density. The accuracy of ECDA is examined by patching the exact exchange (EXX) and the random phase approximation (RPA) correlation energy densities in a one-dimensional hydrogen chain, as well as by patching EXX energy densities in several molecules. The agreement between ECDA and KS-DFT on total energies,

dipole moments, XC potentials, and KS eigenvalues is good in general as the clusters are made larger. Based on these encouraging results, we expect ECDA to be a simple, yet effective method to scale up high-level KS-DFT simulations in large systems.

1 Introduction

Kohn-Sham density functional theory (KS-DFT)[1,2] is widely used for electronic structure simulations. Its accuracy is determined by the approximation for the exchange-correlation (XC) functional, and can be improved by developing high-level XC functionals.[3] High-level XC functionals, such as the random phase approximation (RPA) correlation functional based on the adiabatic-connection fluctuation and dissipation theorem (ACFDT)[4–12] and the *ab initio* XC functionals built based on correlated wave function methods,[13,14] were actively developed in the past. A recent ACFDT functional with a fitted XC kernel reached the accuracy of the couple cluster theory for predicting reaction energies of molecules.[15] Unfortunately, high-level XC functionals often have high computational cost and steep computational scaling, which hinders their application to large systems.

To scale up high-level KS-DFT calculations, we often exploit the idea of the nearsightedness of electronic matter (NEM), which states that the electron correlation at a spatial point $\vec{r}$ is mainly determined by its local information, such as, the electron density and density matrix surrounding $\vec{r}$, with the system's chemical potential kept fixed.[16,17] NEM does not hold in general, however was shown to be valid in various metallic and insulating model systems.[18] NEM has long been used to develop low-scaling correlated wave-function methods.[19–23] The idea of NEM has also been used to develop many other local correlation methods. In Yang's divide-and-conquer method,[24] a system's KS band energy was constructed based on locally calculated KS band energies. In the charge-patching method,[25] a system's electron density is obtained by patching locally computed electron densities. For the subsystem functional method, a region is treated by an XC functional tailored for that region.[26–28] For the many-electron expansion method,[29] a system's energy is systemically improved by computing the energies of n-electron densities based on the energies of $(n-1)$-electron densities. In the density matrix embedding theory,[23] the active space of impurity+bath is defined using the Schmidt decomposition, which yields an active space of a size that is twice of the size of the impurity. The local correlation energy was then calculated and patched over the sys-

tem.[30] In the framework of the reduced density matrix functional theory, a local correlation method based on inverting local reduced density matrices was also developed.[31] The idea of local correlation was also exploited to develop linear scaling algorithms for computing exact exchange (EXX) energy[32] and RPA correlation energy.[33–35]

In this work, we develop a local correlation method in the framework of KS-DFT to directly calculate the XC energy of a large system with an atom-by-atom patching scheme. The method is termed "embedded cluster density approximation" (ECDA) which can be considered as a natural extension of the local density approximation[2] (LDA). Local embedding methods have been actively developed to investigate the region of interest in large systems with high-level methods, with the rest of the system treated by appropriate, low-cost methods. The region of interest can be defined by partitioning the system's electron density[36–49] and density matrix.[23,50–53] With ECDA, we aim to obtain accurate electronic structures in the entire system by performing embedding calculations on all the atoms and stitching the embedding results over the system seamlessly. In our recent XC potential patching method (XCPP),[54] a system's XC energy was also obtained by patching atomic XC energy densities. The main difference between ECDA and XCPP is how to compute the system's XC potential. In XCPP, the XC potential of a cluster is calculated and is then truncated to only keep the part (called atomic XC potential) on the cluster's central atom. The obtained atomic XC potentials were stitched together to obtain the system's XC potential. One drawback with that approach is that the accuracy of these atomic XC potentials is affected by the clusters' boundaries. That drawback is completely avoided by ECDA in which the system's XC potential is computed by directly taking the functional derivative of the system's patched XC energy with respect to the system's electron density.

Some features of ECDA are listed below. The clusters are embedded in the system using the finite-temperature density functional embedding theory (FT-DFET),[55] which ensures that the partitioning of the system's electron density among a cluster and its environment is unique[42,45,55] and does not require the use of locally supported basis functions, such as Gaus-

sian functions. Therefore, ECDA can work with delocalized basis functions, such as plane-wave basis functions. ECDA is applicable to non-metallic, metallic, and finite-temperature quantum systems, as long as NEM holds in these systems. To calculate a cluster's XC energy density, its electron density is required to be v-representable. This is guaranteed in ECDA in which a cluster's electron density, defined with FT-DFET, is always v-representable by construction.

The paper is organized as follows. We discuss how to define embedded clusters based on FT-DFET. We then construct the system's XC energy by patching these locally computed, high-level XC energy densities in an atom-by-atom manner. We derive the relationship between the embedding potentials and the system's KS potential, based on which we show how to efficiently compute the system's XC potential using the first-order perturbation theory. The steps of performing ECDA calculations are then given. The accuracy of ECDA is investigated by patching EXX+RPA energy densities in a one-dimensional H_{20} chain and by patching EXX energy densities in three molecules (ester, Cl-tetracene, and tripeptide).

2 Theoretical Methods

2.1 Define embedded clusters

The first step in ECDA is to group atoms to define clusters for each atom. Taking the atom j for example, we select its neighbors up to N_b bonds away to define its cluster, termed "cluster j". The rest atoms are grouped to define the environment j. The atom j is called the central atom.

For each atom, we calculate its Becke weight.[56] The weight of the atom j is defined as

$$w_j(\mathbf{r}) = \frac{P_j(\mathbf{r})}{\sum_{i=1}^{N_{atom}} P_i(\mathbf{r})}. \tag{1}$$

with the cell function $P_i(\mathbf{r}) = \prod_{j \neq i} s_{ij}(\mathbf{r})$. s_{ij} is the switching function defined based on

$h_{ij}(\mathbf{r})$ that measures the relative position of a point $\mathbf{r}$ to two atoms i and j

$$h_{ij}(\mathbf{r}) = \frac{|\mathbf{R}_i - \mathbf{r}| - |\mathbf{R}_j - \mathbf{r}|}{|\mathbf{R}_i - \mathbf{R}_j|}, \tag{2}$$

where $\mathbf{R}_i$ and $\mathbf{R}_j$ are the coordinates of atoms i and j, respectively. Becke defined $s_{ij}(\mathbf{r}) = (1 - f_3(h_{ij}(\mathbf{r})))/2$ recursively with $f_1(x) = x(3 - x^2)/2$ and $f_k(x) = f_1(f_{k-1}(x))$. To obtain softer weights that are easier to be represented on a uniform grid, we set $s_{ij}(\mathbf{r}) = (1 - f_1(h_{ij}(\mathbf{r})))/2$.

The weights of the cluster j and the environment j are the sum of the weights of the atoms in the cluster and environment, respectively,

$$w_{clu,j}(\mathbf{r}) = \sum_n w_n(\mathbf{r}) \tag{3}$$

$$w_{env,j}(\mathbf{r}) = \sum_m w_m(\mathbf{r}), \tag{4}$$

where n and m run over the atoms in the cluster and the environment, respectively.

2.2 Partition the system's electron density among the clusters and their environments

We now proceed to partition the system's electron density among the cluster j and its environment. First, we define their regions by partitioning the system's KS potential v_{KS} as

$$v_{clu,j}(\mathbf{r}) = w_{clu,j}(\mathbf{r})v_{KS}(\mathbf{r}) + (1 - w_{clu,j}(\mathbf{r}))(\mu + v_b) \tag{5}$$

$$v_{env,j}(\mathbf{r}) = w_{env,j}(\mathbf{r})v_{KS}(\mathbf{r}) + (1 - w_{env,j}(\mathbf{r}))(\mu + v_b), \tag{6}$$

where μ is the system's chemical potential. We note that $v_{clu,j}$ and $v_{env,j}$ reach a potential plateau of the height of $\mu + v_b$ at distant. Due to the inclusion of μ in above definitions, this potential plateau is always higher than the system's chemical potential by v_b. With a

relatively large v_b (which is set to 0.5 a.u. in this work), $v_{clu,j}$ and $v_{env,j}$ confine the cluster and the environment's electron densities.

We employ FT-DFET[55] to partition the system's electron density, such that, the sum of the cluster and the environment densities matches the system's density $\rho_{tot}(\mathbf{r})$

$$\rho_{clu,j}(\mathbf{r}) + \rho_{env,j}(\mathbf{r}) = \rho_{tot}(\mathbf{r}). \tag{7}$$

This condition is realized by applying an appropriate embedding potential $v_{emb,j}$ to both the cluster and its environment. The cluster and the environment's KS potentials become

$$v_{KS}^{clu,j}(\mathbf{r}) = v_{clu,j}(\mathbf{r}) + v_{emb,j}(\mathbf{r}) \tag{8}$$

$$v_{KS}^{env,j}(\mathbf{r}) = v_{env,j}(\mathbf{r}) + v_{emb,j}(\mathbf{r}). \tag{9}$$

$\rho_{clu,j}(\mathbf{r})$ and $\rho_{env,j}(\mathbf{r})$ in Eq. 7 are obtained by solving the KS equation with the above KS potentials $v_{KS}^{clu,j}$ and $v_{KS}^{env,j}$, respectively. To solve for $v_{emb,j}$ that makes Eq. 7 hold, we extend the Zhao-Parr method[57–59] to two quantum systems by adding a penalty function C_λ

$$C_\lambda = \lambda \frac{1}{2} \iint d\mathbf{r} d\mathbf{r}' \Delta\rho(\mathbf{r}) \Delta\rho(\mathbf{r}') \frac{\mathrm{erfc}(\eta|\mathbf{r}-\mathbf{r}'|)}{|\mathbf{r}-\mathbf{r}'|} \tag{10}$$

to the KS Hamiltonians of the cluster and its environment, with

$$\Delta\rho(\mathbf{r}) = \rho_{clu,j}(\mathbf{r}) + \rho_{env,j}(\mathbf{r}) - \rho_{tot}(\mathbf{r}). \tag{11}$$

The Coulomb operator in Eq. 10 is screened by the complementary error function to avoid the charge sloshing[60] that makes the convergence of $v_{emb,j}$ slow. A screening length η of 3 Å works well in our calculations. The penalty term introduces a penalty potential

$$v_P^\lambda(\mathbf{r}) = \lambda \int d\mathbf{r}' \Delta\rho(\mathbf{r}') \frac{\mathrm{erfc}(\eta|\mathbf{r}-\mathbf{r}'|)}{|\mathbf{r}-\mathbf{r}'|} \tag{12}$$

to the cluster and environment's KS equations

$$\Big(-\frac{1}{2}\nabla^2 + v_{clu,j} + v_P^{\lambda}\Big)\phi_n^{clu,j} = \epsilon_n^{clu,j}\phi_n^{clu,j} \tag{13}$$

$$\Big(-\frac{1}{2}\nabla^2 + v_{env,j} + v_P^{\lambda}\Big)\phi_n^{env,j} = \epsilon_n^{env,j}\phi_n^{env,j}, \tag{14}$$

where $\phi_n^{clu,j}$ and $\phi_n^{env,j}$ are the n-th KS orbitals of the cluster j and the environment j, respectively. $\epsilon_n^{clu,j}$ and $\epsilon_n^{env,j}$ are the KS eigenvalues. Eqs. 13 and 14 are solved with the numbers of electrons in the cluster and the environment specified as

$$N_{clu,j} = \int d\mathbf{r}'\rho_{tot}(\mathbf{r}')w_{clu,j}(\mathbf{r}') \tag{15}$$

$$N_{env,j} = \int d\mathbf{r}'\rho_{tot}(\mathbf{r}')w_{env,j}(\mathbf{r}'). \tag{16}$$

After solving Eqs. 13 and 14, the cluster and the environment's densities are obtained as

$$\rho_{clu,j}(\mathbf{r}) = 2\sum_n f_n^{clu,j}(\phi_n^{clu,j}(\mathbf{r}))^2 \tag{17}$$

$$\rho_{env,j}(\mathbf{r}) = 2\sum_n f_n^{env,j}(\phi_n^{env,j}(\mathbf{r}))^2, \tag{18}$$

where $f_n^{clu,j}$ and $f_n^{env,j}$ are the occupation numbers. v_P^{λ} is obtained by solving the coupled equations 12, 13, and 14. As $\lambda \to \infty$, $\Delta\rho \to 0$ and $v_P^{\lambda}(\mathbf{r})$ becomes the embedding potential $v_{emb,j}(\mathbf{r})$.

2.3 Construct the system's exchange-correlation energy through an atom-by-atom patching

After the density partitioning, the cluster j's XC energy density $\varepsilon_{xc}^{clu,j}(\mathbf{r})$, by integrated which we obtain the cluster's XC energy, is computed based on its KS orbitals. The atomic XC

energy of the atom j is obtained as

$$E_{xc}^{atom,j} = \int d^3r' \varepsilon_{xc}^{clu,j}(\mathbf{r}')w_j(\mathbf{r}'), \tag{19}$$

based on which the system's XC energy is constructed through an atom-by-atom patching scheme

$$E_{xc} = \sum_{n=1}^{N_{atom}} E_{xc}^{atom,n} \tag{20}$$

where n runs over all the atoms. In this work, we patch EXX and RPA correlation energy densities in a 1D hydrogen chain and patch EXX energy density in several molecules.

There are two popular definitions for EXX: one is based on the Hartree-Fock (HF) exchange and another one is based on ACFDT. The HF EXX is defined as

$$E_x^{HF} = -\sum_{ij} f_i f_j \iint d^3r d^3r' \frac{\psi_i(\mathbf{r})\psi_j(\mathbf{r})\psi_j(\mathbf{r}')\psi_i(\mathbf{r}')}{|\mathbf{r}-\mathbf{r}'|}. \tag{21}$$

The ACFDT EXX is defined as[61]

$$E_x^{EXX} = -\sum_{ij} f_i c_{ij} \iint d^3r d^3r' \frac{\psi_i(\mathbf{r})\psi_j(\mathbf{r})\psi_j(\mathbf{r}')\psi_i(\mathbf{r}')}{|\mathbf{r}-\mathbf{r}'|}, \tag{22}$$

where $c_{ij} = 1 + \mathrm{sgn}(\epsilon_i - \epsilon_j)$ and $\{\epsilon_i\}$ are the KS eigenvalues. These two definitions are identical if the occupation numbers $\{f_i\}$ are integers, i.e., either 0 or 1.

In ECDA, we employ ACFDT EXX to calculate the clusters' EXX energy densities, since the obtained clusters' XC energy densities better approximate the system's EXX energy density. The reason for not using HF EXX is that a cluster's exchange holes $n_x(\mathbf{r}, \mathbf{r}')$, defined based on HF EXX, do not obey the sum rule ($\int d^3r' n_x(\mathbf{r}, \mathbf{r}') = -1$), if the cluster's KS orbitals are fractionally occupied.[62] On the other hand, clusters defined with FT-DFET often have fractionally occupied KS orbitals. The system's exchange holes which satisfy the sum rule then cannot be well approximated by the clusters' exchange energy densities defined

based on HF EXX. This problem is avoided by computing clusters' EXX energy densities based on ACFDT EXX, since exchange holes defined based on ACFDT EXX always satisfy the sum rule,[63] no matter the occupation numbers are fractional or integral. We define the energy density of ACFDT EXX as

$$\varepsilon_x^{EXX}(\mathbf{r}) = -\sum_{ij} f_i c_{ij} \psi_i(\mathbf{r}) \psi_j(\mathbf{r}) \int d\mathbf{r}_2 \frac{\psi_i(\mathbf{r}_2)\psi_j(\mathbf{r}_2)}{|\mathbf{r}-\mathbf{r}_2|}. \tag{23}$$

To define RPA correlation energy density, we start with the RPA correlation energy

$$E_c^{RPA} = \frac{1}{2\pi} \int_0^\infty d\omega \mathrm{Tr}[\ln(1 - V_{coul} X_0(i\omega)) + V_{coul} X_0(i\omega)], \tag{24}$$

V_{coul} is the matrix representation of the Coulomb potential $v_{coul}(\mathbf{r}, \mathbf{r}') = 1/|\mathbf{r}-\mathbf{r}'|$ in the basis of grid points. $X_0(i\omega)$ is the KS linear response function $\chi_0(\mathbf{r}, \mathbf{r}'; i\omega)$ (at an imaginary frequency $i\omega$) represented in the basis of grid points. We define RPA correlation energy density at the grid point j

$$\varepsilon_c^{RPA}(\mathbf{r}_j) = \frac{1}{2\pi\Delta V} \int_0^\infty d\omega M_{j,j}(i\omega) \tag{25}$$

where ΔV is the volume element and $M_{j,j}$ denotes the (j,j)-th element of the matrix M

$$M(i\omega) = \ln(I - V_{coul}^{1/2} X_0(i\omega) V_{coul}^{1/2}) + V_{coul}^{1/2} X_0(i\omega) V_{coul}^{1/2}. \tag{26}$$

2.4 Calculate the system's exchange-correlation potential

The system's XC potential $v_{xc}(\mathbf{r})$ is calculated by solving the optimized effective potential (OEP) equation[64–67]

$$\begin{aligned} \frac{\delta E_{xc}}{\delta v_{KS}(\mathbf{r})} &= \int d\mathbf{r}' v_{xc}(\mathbf{r}') \frac{\delta \rho_{tot}(\mathbf{r}')}{\delta v_{KS}(\mathbf{r})} \\ &= \int d\mathbf{r}' v_{xc}(\mathbf{r}') \chi_0(\mathbf{r}, \mathbf{r}'), \end{aligned} \tag{27}$$

where $\chi_0(\mathbf{r},\mathbf{r}')$ is the system's KS linear response function.

To solve for $v_{xc}(\mathbf{r})$, we need $\delta E_{xc}/\delta v_{KS}(\mathbf{r})$. First, we show that this derivative exists. The proof is based on our recent proof that, for a KS system at finite temperature, the mapping between its KS potential and the embedding potential is one-to-one.[55] Therefore, $v_{emb,j}$ is a functional of v_{KS}. On the other hand, the cluster j's electron density $\rho_{clu,j}$ is a functional of v_{KS} and $v_{emb,j}$, and therefore $\rho_{clu,j}$ is a functional of v_{KS} only. E_{xc} is a functional of the electron densities of all clusters; therefore, E_{xc} is a functional of v_{KS}. This proves that the derivative $\delta E_{xc}/\delta v_{KS}(\mathbf{r})$ exists.

We then have

$$\frac{\delta E_{xc}}{\delta v_{KS}(\mathbf{r})} = \sum_{j=1}^{N_{atom}} \int d\mathbf{r}' w_j(\mathbf{r}') \frac{\delta \varepsilon_{xc}^{clu,j}(\mathbf{r}')}{\delta v_{KS}(\mathbf{r})}. \tag{28}$$

To compute $\delta \varepsilon_{xc}^{clu,j}(\mathbf{r}')/\delta v_{KS}(\mathbf{r})$, we fix the number of electrons ($N_{clu,j}$) in the cluster j and also fix the system's chemical potential μ in the definition of $v_{clu,j}(\mathbf{r})$ (Eq. 5). If we do not fix μ, the interaction between the system's KS potential $v_{KS}(\mathbf{r})$ and $\varepsilon_{xc}^{clu,j}(\mathbf{r}')$ will be of long range, which violates NEM. To explain this, we note that any change in v_{KS} at distant will cause a change in μ which in turn will cause a change in $v_{clu,j}(\mathbf{r})$. $v_{clu,j}(\mathbf{r})$ will then cause a change in the cluster j's XC energy density.

By fixing $N_{clu,j}$ and μ, $\varepsilon_{xc}^{clu,j}$ is a functional of $v_{KS}^{clu,j}$, and we have, by the chain rule,

$$\frac{\delta \varepsilon_{xc}^{clu,j}(\mathbf{r}')}{\delta v_{KS}(\mathbf{r})} = \int d\mathbf{r}_1 \frac{\delta \varepsilon_{xc}^{clu,j}(\mathbf{r}')}{\delta v_{KS}^{clu,j}(\mathbf{r}_1)} \frac{\delta v_{KS}^{clu,j}(\mathbf{r}_1)}{\delta v_{KS}(\mathbf{r})}, \tag{29}$$

With $v_{KS}^{clu,j}$ defined in Eq. 8, we have (with μ kept fixed)

$$\frac{\delta v_{KS}^{clu,j}(\mathbf{r}_1)}{\delta v_{KS}(\mathbf{r})} = w_{clu,j}(\mathbf{r})\delta(\mathbf{r}-\mathbf{r}_1) + \frac{\delta v_{emb,j}(\mathbf{r}_1)}{\delta v_{KS}(\mathbf{r})} \tag{30}$$

Combining equations 29, 30, and 28, we have

$$\frac{\delta E_{xc}}{\delta v_{KS}(\mathbf{r})} = p_1(\mathbf{r}) + p_2(\mathbf{r}), \tag{31}$$

with

$$p_1(\mathbf{r}) = \sum_{j=1}^{N_{atom}} y_j(\mathbf{r}) w_{clu,j}(\mathbf{r}) \tag{32}$$

$$p_2(\mathbf{r}) = \sum_{j=1}^{N_{atom}} \int d\mathbf{r}_1 y_j(\mathbf{r}_1) \frac{\delta v_{emb,j}(\mathbf{r}_1)}{\delta v_{KS}(\mathbf{r})}, \tag{33}$$

where y_j is defined

$$y_j(\mathbf{r}) = \int d\mathbf{r}' w_j(\mathbf{r}') \frac{\delta \varepsilon_{xc}^{clu,j}(\mathbf{r}')}{\delta v_{KS}^{clu,j}(\mathbf{r})}. \tag{34}$$

$p_1(\mathbf{r})$ accounts for the change of the clusters' XC energy densities due to the change of the system's KS potential with the embedding potentials fixed. $p_2(\mathbf{r})$ accounts for the change of the clusters' XC energy densities due to the change of the embedding potentials with the system's KS potential fixed. To compute y_i, we need to compute $\delta \varepsilon_{xc}^{clu,j} / \delta v_{KS}^{clu,j}$. The analytical expression of y_j for ACFDT EXX is given in Appendix A. For RPA correlation energy, $\delta \varepsilon_{c,RPA}^{clu,j}(\mathbf{r}) / \delta v_{KS}^{clu,j}(\mathbf{r}')$ is calculated using the central finite difference in the MATLAB code by perturbing $v_{KS}^{clu,j}(\mathbf{r})$ at each grid point by ± 0.001 a.u.. $\varepsilon_{c,RPA}^{clu,j}(\mathbf{r})$ is the RPA correlation energy density of cluster j.

Now, the task is to efficiently calculate $p_2(\mathbf{r})$ without explicitly computing $\delta v_{emb,j} / \delta v_{KS}$. We first derive the connection between $v_{emb,j}$ and v_{KS}. By perturbing v_{KS}, the system's density ρ_{tot} changes as

$$\delta \rho_{tot}(\mathbf{r}) = \int d\mathbf{r}' \chi_0(\mathbf{r}, \mathbf{r}') \delta v_{KS}(\mathbf{r}'). \tag{35}$$

The embedding potential $v_{emb,j}$ is adjusted such that the sum of the cluster and environment's electron densities still matches the system's density

$$\begin{aligned} \delta \rho_{tot}(\mathbf{r}) &= \delta \rho_{clu,j}(\mathbf{r}) + \delta \rho_{env,j}(\mathbf{r}) \\ &= \int d\mathbf{r}' \chi_0^{clu,j}(\mathbf{r}, \mathbf{r}') \delta v_{KS}^{clu,j}(\mathbf{r}') + \int d\mathbf{r}' \chi_0^{env,j}(\mathbf{r}, \mathbf{r}') \delta v_{KS}^{env,j}(\mathbf{r}') \end{aligned} \tag{36}$$

with

$$\delta v_{KS}^{clu,j}(\mathbf{r}) = \delta v_{emb,j}(\mathbf{r}) + w_{clu,j}(\mathbf{r})\delta v_{KS}(\mathbf{r}) \tag{37}$$

$$\delta v_{KS}^{env,j}(\mathbf{r}) = \delta v_{emb,j}(\mathbf{r}) + w_{env,j}(\mathbf{r})\delta v_{KS}(\mathbf{r}). \tag{38}$$

Same to the derivation of Eq. 28, above variations are performed with cluster j's electron number and chemical potential kept fixed. Combining equations 35, 36, 37, and 38, we obtain

$$\begin{aligned}\frac{\delta v_{emb,j}(\mathbf{r})}{\delta v_{KS}(\mathbf{r}')} &= \int d\mathbf{r}''(\chi_0^{clu,j} + \chi_0^{env,j})^{-1}(\mathbf{r},\mathbf{r}'') \\ &\times[\chi_0(\mathbf{r}'',\mathbf{r}') - \chi_0^{clu,j}(\mathbf{r}'',\mathbf{r}')w_{clu,j}(\mathbf{r}') - \chi_0^{env,j}(\mathbf{r}'',\mathbf{r}')w_{env,j}(\mathbf{r}')]\end{aligned} \tag{39}$$

Inserting Eq. 39 to Eq. 33 and defining

$$z_j(\mathbf{r}) = \int d^3r' y_j(\mathbf{r}')(\chi_0^{clu,j} + \chi_0^{env,j})^{-1}(\mathbf{r}',\mathbf{r}), \tag{40}$$

$p_2(\mathbf{r})$ becomes

$$p_2(\mathbf{r}) = \sum_{j=1}^{N_{atom}} \int d^3r' z_j(\mathbf{r}')[\chi_0(\mathbf{r}',\mathbf{r}) - \chi_0^{clu,j}(\mathbf{r}',\mathbf{r})w_{clu,j}(\mathbf{r}) - \chi_0^{env,j}(\mathbf{r}',\mathbf{r})w_{env,j}(\mathbf{r})]. \tag{41}$$

To avoid inverting the KS linear responses in Eq. 40, z_j is obtained by solving the linear system

$$\int d^3r'[\chi_0^{clu,j}(\mathbf{r},\mathbf{r}') + \chi_0^{env,j}(\mathbf{r},\mathbf{r}')]z_j(\mathbf{r}') = y_j(\mathbf{r}) \tag{42}$$

using conjugate gradient method. The product between a KS linear response function and a vector is calculated by solving the Sternheimer equation derived for KS systems with fractionally occupied KS orbitals.[68] This is necessary for ECDA, because clusters' KS orbitals are often fractionally occupied. After obtaining z_j, p_2 is also calculated by solving the Sternheimer equation without explicitly constructing these KS linear response functions in

Eq. 41.

To summarize, the steps of performing ECDA calculations are:

Step 1: Solve the system's KS equation with a KS potential $v_{KS}(\mathbf{r})$. For the initial guess, we set v_{KS} to the KS potential from a converged KS-DFT-LDA calculation. Obtain the system's electron density $\rho_{tot}(\mathbf{r})$. Update the numbers of electrons in clusters and environments based on Eqs. 15 and 16. Update $\{v_{clu,j}(\mathbf{r})\}$ and $\{v_{env,j}(\mathbf{r})\}$ with $v_{KS}(\mathbf{r})$ and the system's chemical potential μ.

Step 2: Select an atom j. Partition the system's electron density among its cluster and the environment based on FT-DFET.[55] Calculate the cluster's XC energy density using a high-level XC functional.

Step 3: Repeat Step 2 for all the atoms.

Step 4: Calculate the system's XC energy via the atom-by-atom patching (Eqs. 20 and 19). Compute $\delta E_{xc}/\delta v_{KS}$ based on which we calculate the system's XC potential $v_{xc}(\mathbf{r})$ by solving the OEP equation 27. Update $v_{KS}(\mathbf{r})$. If $v_{KS}(\mathbf{r})$ is not converged, go back to Step 1. In practice, the convergence of v_{KS} is accelerated by Pulay mixing.[69]

2.5 Extend the application scope of ECDA by treating the Kohn-Sham systems of the system, clusters, and environments at finite temperature

In ECDA, the system's KS orbitals are fractionally occupied according to the Fermi-Dirac (F-D) statistics at temperature T. This is important for ECDA to be applicable to a wide range of materials. The reason is that the electron density of a quantum system having static correlation cannot be represented by a pure-state density (formed by KS orbitals with integral occupation numbers) without violating the Aufbau principle.[70–73] A system's electron density is called non-interacting ensemble v-representable (EVR), if its KS orbitals are occupied

following F-D statistics.[74] It was hypothesized that the mapping between interacting EVR densities and non-interacting EVR densities is one-to-one.[74] This hypothesis was, at least, true for lattice quantum systems.[75] If this hypothesis is true in general, by treating the system's KS system at finite temperature, ECDA is applicable to a wide range of interacting electronic systems. In addition, in ECDA we also treat clusters' and environments' KS systems at the same temperature T.

We point out that the temperature T is only used to generate non-interacting EVR densities. The clusters' XC energy densities are still computed using the XC functionals constructed for zero-temperature electron systems. Therefore, in practice we need to set T low enough to make it valid to employ these zero-temperature XC functionals. Note that ECDA is also applicable to systems at finite temperature. We just need to set T to that temperature and employ finite-temperature XC functionals[76–78] to compute clusters' XC energy densities.

3 Numerical details

In all ECDA calculations, KS orbitals of the systems, clusters, and environments are occupied according to the Fermi-Dirac statistics, with a smearing temperature of 0.05 eV unless specified. ECDA is implemented in a 1D KS-DFT program implemented in MATLAB.[79] Details of this 1D KS-DFT program was given in Ref.[80]. The performance of ECDA is investigated on a bond-alternating H_{20} chain. The lengths of the short and long bonds are 1.8 bohr and 2.644 bohr, respectively, and therefore covalent bonds are formed in an alternating manner. LDA XC functional for one-dimensional systems are taken from Ref.[81] and Ref.[82]. A soft Coulomb potential $v_{coul}(x,x') = 1/\sqrt{a+(x-x')^2}$ with $a = 1.0$ bohr is used to describe the electron-electron and ion-electron interactions. The nuclear charge of the pseudo H atom is 1.2. A grid spacing of 0.33 bohr is used in all calculations, which converges KS-DFT-LDA energies to better than 0.1 mHa/atom. To compute the RPA correlation energy, the integral

over frequency is evaluated with Gauss-Legendre quadrature with 15 nodes. The maximum frequency is set to 10 a.u.. To partition the system's electron density among a cluster and its environment, we use the extended Wu-Yang method developed in our previous work.[55,83]

We also implement ECDA in the ABINIT program.[84] We perform ECDA-EXX calculations on several molecules. Their geometries are relaxed by ABINIT using the Perdew-Burke-Ernzerhof XC functional.[85] ECDA calculations are performed with a relatively small kinetic energy cutoff of 600 eV to reduce the computational cost of solving the Sternheimer equation[68] and EXX calculations. For the calculations of bond energies and bond rotation energies, a 400 eV kinetic energy cutoff is used to further reduce the computational cost of ECDA. EXX energy and its potential are calculated in real space by computing the integral $\int dr'^3 \phi_i(\mathbf{r}')\phi_j(\mathbf{r}')/|\mathbf{r}-\mathbf{r}'|$ using the Poisson solver implemented in ABINIT.[86,87] To partition a system's electron density among a cluster and its environment, we employ the modified Zhao-Parr method discussed in Section 2.2. Eq. 12 is efficiently calculated with plane wave basis functions.[88] v_P^λ is obtained by solving the coupled equations 12, 13, and 14, and the convergence is accelerated by using Pulay mixing.[69] The contour plots of EXX potentials are produced using VESTA.[89] The details of solving the OEP equation 27 and Eq. 42 are given in the Supporting Information.

4 Results and discussions

4.1 ECDA-RPA calculations of a bond-alternating, one-dimensional hydrogen chain

In ECDA, it is required that the system's electron density matches the cluster's electron density inside a cluster, that is, $\rho_{clu}(\mathbf{r}) \to \rho_{tot}(\mathbf{r})$ for $\mathbf{r}$ deep inside the cluster. This is observed in Fig. 1(a) which shows the partitioning of the electron density of H_{20} among a cluster and its environment. The cluster is defined for the atom #10 by including its neighboring atoms up to the second nearest neighbors to define the cluster. We find that

the cluster's electron density matches the system's density inside the cluster. Furthermore, the cluster's and the environment's densities are well localized in their regions due to the potential plateau ($\mu + v_b$) from $v_{clu,j}$ and $v_{env,j}$ (Eqs. 5 and 6). The embedding potential for this partitioning is given in Fig. 1(b). It fluctuates mostly at the interfaces between the cluster and the environment. The reason is that the density matching condition (Eq. 7) can hold inside the cluster and the environment without much help from the embedding potential. This is due to the fact that $v_{clu,j}$ and $v_{env,j}$ match the system's KS potential inside the cluster and the environment, respectively.

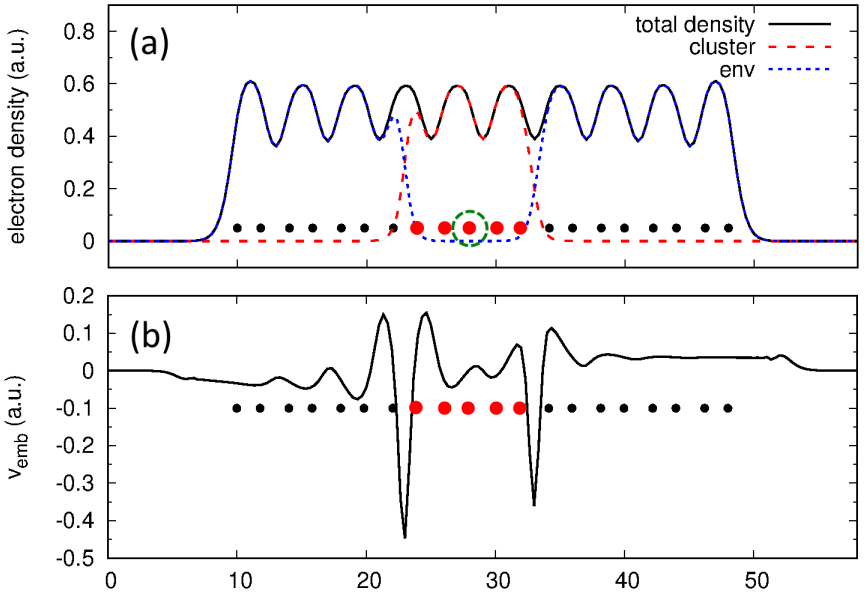

Figure 1: (a) Partitioning of H_{20}'s electron density among the cluster (larger red dots) and its environment (smaller black dots). The cluster is defined for the atom #10 (marked by the green dashed circle). (b) The embedding potential for this density partitioning.

The accuracy of ECDA is assessed by performing ECDA-RPA calculations on this 1D H chain: The EXX and RPA correlation energy densities are patched over the chain to construct the system's EXX+RPA energy. Fig. 2 gives the energies for stretching the H_{19}-H bond. The benchmark is from self-consistent KS-DFT-RPA calculations. ECDA-RPA calculations are performed self-consistently using different cluster sizes. With $N_b = 2$, the errors per atom are below 6 mHa for all bond lengths. As we increase the cluster sizes, the

errors decrease quickly, however in a zigzag way (Fig. 3). We believe that this zigzag behavior of convergence is an intrinsic property of density partitioning. This zigzag convergence was also observed in Ref.[90] in which Yang's divide-and-conquer method was used to patch the Hartree-Fock energy in molecules.

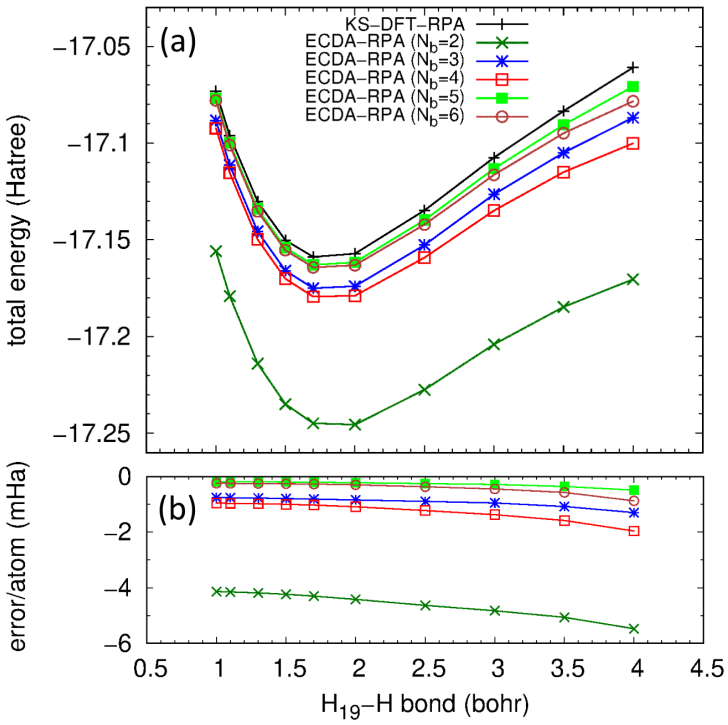

Figure 2: Energy curves for stretching the H_{19}-H bond from self-consistent KS-DFT-RPA and self-consistent ECDA-RPA (with N_b =2, 3, and 4) calculations.

A stringent test of the accuracy of ECDA is to compare the XC potentials from self-consistent ECDA-RPA and self-consistent KS-DFT-RPA (benchmarks) calculations. The results are given in Fig. 4. ECDA XC potentials agree reasonably with the benchmarks, except that the fluctuation of ECDA XC potentials is less. ECDA XC potentials are improved as we make the clusters larger, however, again in a zigzag manner. We observe an error cancellation between ECDA's EXX and ECDA's RPA potentials: Wherever ECDA's EXX potential is higher/lower than the benchmarks, ECDA's RPA potential is lower/higher than the benchmarks. This error cancellation is due to the fact that the exchange hole is partially cancelled by the RPA correlation hole as observed in Ref.[80]. EXX+RPA energy is then more

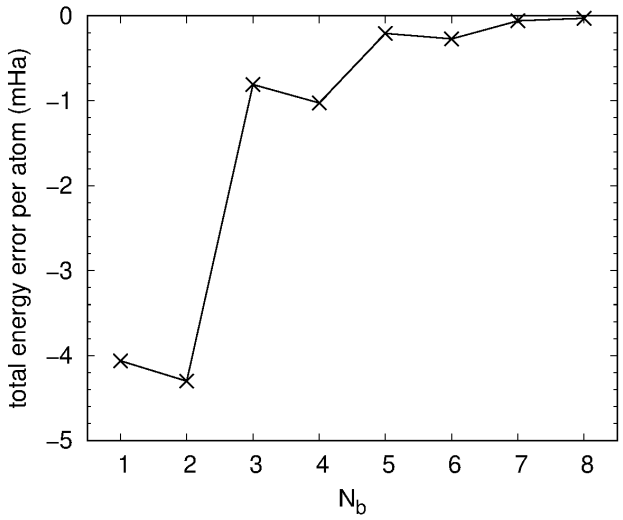

Figure 3: Error in total energy per atom, $(E_{tot}^{ECDA} - E_{tot}^{KS})/N_{atom}$, for different cluster sizes. E_{tot}^{ECDA} and E_{tot}^{KS} are total energies from self-consistent ECDA-RPA and self-consistent KS-DFT-RPA calculations, respectively. The bond length of H19-H is set to 1.7 bohr.

nearsighted than either EXX energy or RPA correlation energy. This suggests that the error in ECDA's EXX+RPA potential is smaller than the error in either ECDA's EXX potential or ECDA's RPA correlation potential. This is the reason for the observed error cancellation between ECDA's EXX and RPA correlation potentials.

Next, we examine the importance of including the dependence of the embedding potential on the system's KS potential in the calculation of the system's XC potential. The system's XC potential is computed based on $\delta E_{xc}/\delta v_{KS}(\mathbf{r})$ which contains two components: $p_1(\mathbf{r})$ and $p_2(\mathbf{r})$ (Eqs. 32 and 33). Fig. 5 shows $p_1(\mathbf{r})$ and $p_2(\mathbf{r})$, and compare $p_1(\mathbf{r}) + p_2(\mathbf{r})$ with the benchmark $\delta E_{xc}^{EXX+RPA}/\delta v_{KS}$. $p_1(\mathbf{r})$, $p_2(\mathbf{r})$, and the benchmarks are all computed based on the KS orbitals from self-consistent ECDA-RPA calculations with $N_b = 3$. Fig. 5 shows that both p_1 and p_2 deviate significantly from the benchmark, however, the sum of them is close to the benchmark. This indicates that both $p_1(\mathbf{r})$ and $p_2(\mathbf{r})$ contribute significantly to $\delta E_{xc}/\delta v_{KS}(\mathbf{r})$. The large contribution from $p_2(\mathbf{r})$ indicates that it is important to consider the dependence of a cluster's XC energy density on its embedding potential (which depends on the system's KS potential) in the calculation of $\delta E_{xc}/\delta v_{KS}$. Such dependence was ignored in our previous XCPP method,[54] in which a cluster's XC potential was calculated with its

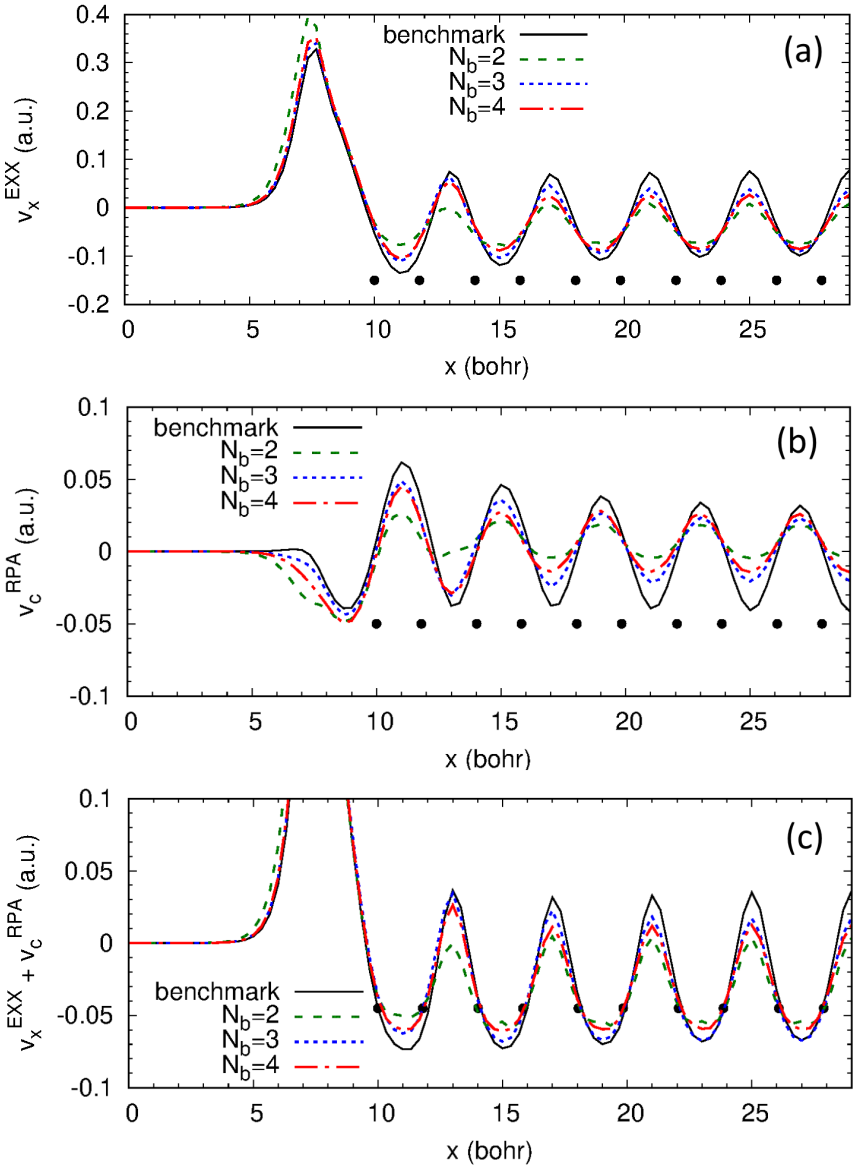

Figure 4: EXX, RPA, and EXX+RPA potentials from non-self-consistent KS-DFT-RPA and non-self-consistent ECDA-RPA calculations. Both calculations are based on the KS orbitals from KS-DFT-LDA calculations. For brevity, only the first ten H atoms are shown due to the symmetry and are marked by the black dots.

embedding potential kept fixed.

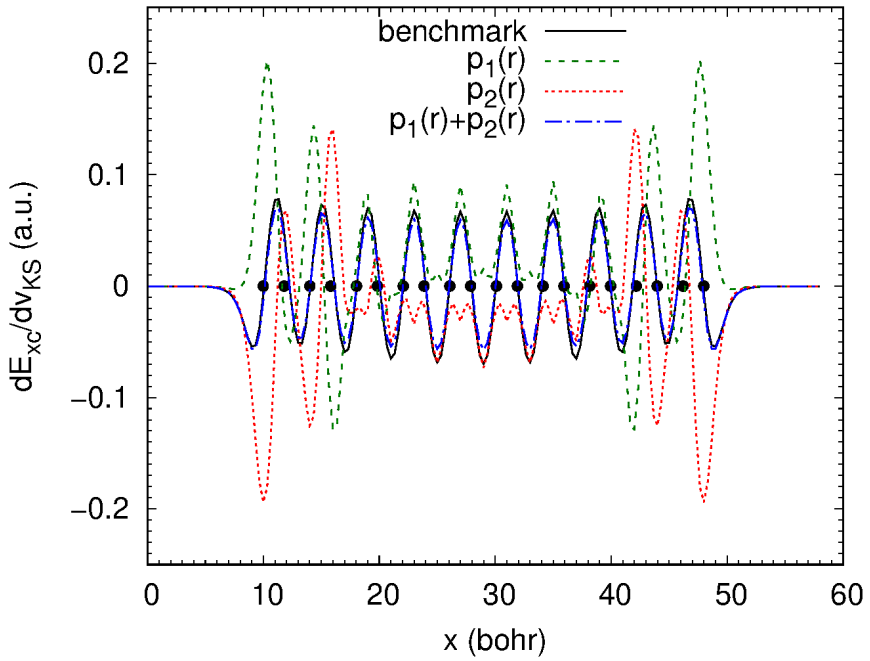

Figure 5: The two components of $\delta E_{xc}/\delta v_{KS}(\mathbf{r})$: $p_1(\mathbf{r})$ and $p_2(\mathbf{r})$. Both are calculated with $N_b = 3$. The sum of them are compared to the benchmark $\delta E_{xc}^{EXX+RPA}/\delta v_{KS}(\mathbf{r})$. H atoms are marked by the black dots.

The accuracy of ECDA-RPA calculations is further assessed by comparing the KS eigenvalues from self-consistent KS-DFT-RPA and self-consistent ECDA-RPA calculations. In Fig. 6, a good agreement between KS-DFT-RPA and ECDA-RPA is observed for both occupied and several lowest unoccupied states. ECDA-RPA predicts a KS gap of 3.19 eV for all cases ($N_b = 2$, 3, and 4), which agree well with the KS gap 3.17 eV from KS-DFT-RPA.

4.2 ECDA-EXX calculations on molecules

The performance of ECDA is also investigated on three molecules by patching their EXX energy densities. The molecules are (a) ester, (b) Cl-tetracene, and (c) tripeptide, with their structures given in Fig. 7. The reason for choosing them is that charge is redistributed in these molecules. For example, in ester, there is a charge transfer between O1 and C1, and between C1 and O2. In Cl-tetracene, there is a charge transfer between C1 and chlorine. In

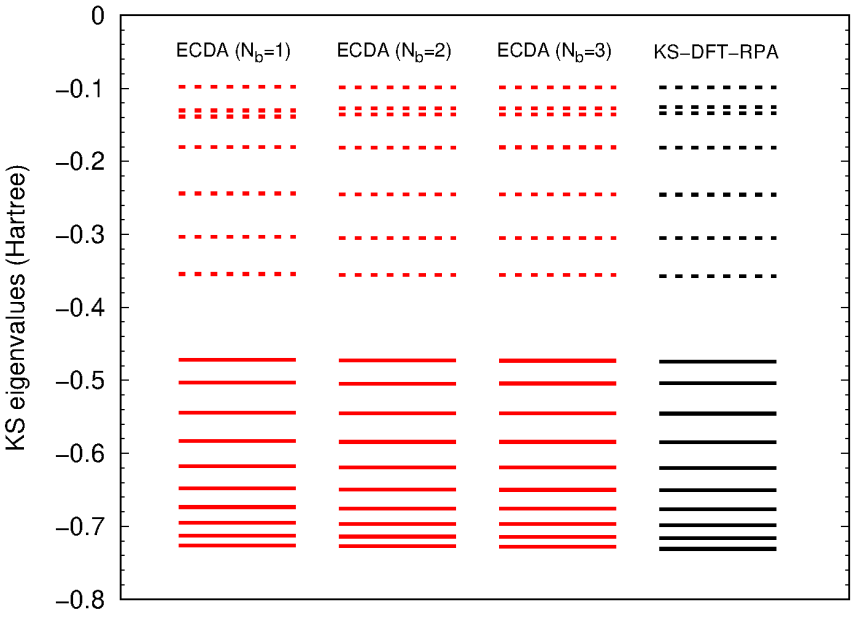

Figure 6: KS eigenvalues from self-consistent KS-DFT-RPA and self-consistent ECDA-RPA (with $N_b = 1$, 2, and 3) calculations.

tripeptide, there is a charge transfer along C-O and N-H bonds. In addition, tripeptide has a large dipole moment along its backbone. Thus, these molecules are good testbeds for investigating ECDA's accuracy for studying heterogeneous systems where charge redistribution takes place.

We first determine the appropriate penalty coefficient λ in the Zhao-Parr method. Table 1 shows the convergence of total energies, dipole moments, and KS gaps with respect to λ. In these ECDA-EXX calculations, the clusters are defined by including the neighboring atoms up to three bonds away (i.e., $N_b = 3$). We note that a very large λ makes the convergence of Zhao-Parr method slow, which is a common problem with penalty methods. Thus, we try to set λ as small as possible. Table 1 shows that for ester and Cl-tetracene $\lambda = 50$ converges the total energies, dipole moments, and KS band gaps within several milliHartrees, 0.1 Debye, and 0.1 eV, respectively; therefore, $\lambda = 50$ is used in their following ECDA-EXX calculations unless specified. For tripeptide, $\lambda = 20$ is used in its later ECDA-EXX calculations.

Table 2 gives the convergence of ECDA-EXX with the cluster sizes. The benchmarks are from self-consistent KS-DFT-EXX calculations. We observe that ECDA energies converge

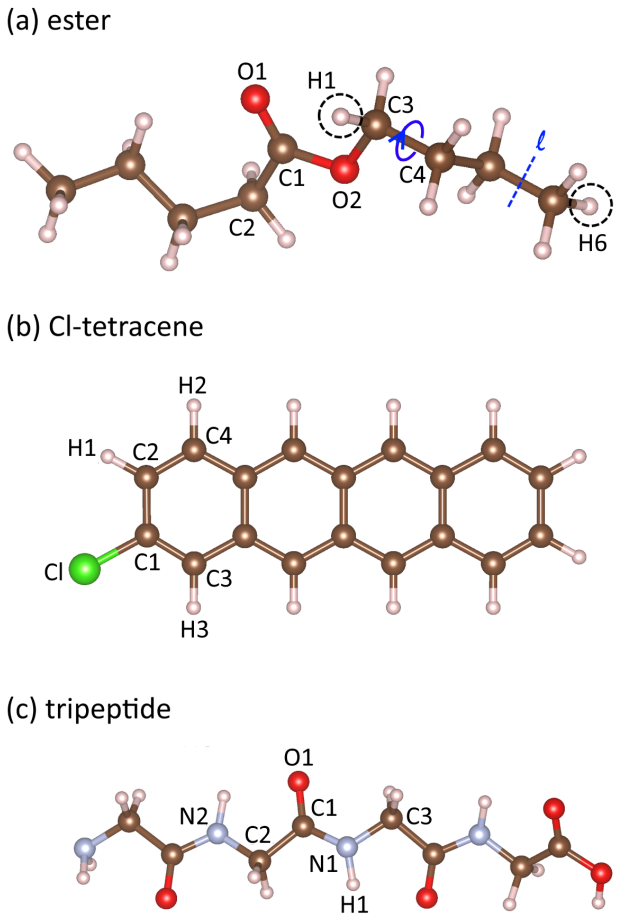

Figure 7: Structures of (a) ester molecule, (b) Cl-tetracene, and (c) tripeptide used for ECDA-EXX calculations. H, C, N, O, S, and Cl atoms are white, brown, light blue, red, yellow and green, respectively.

Table 1: Convergence of total energies (in Hartree), dipole moments (in Debye), and KS gaps (in eV) from self-consistent ECDA-EXX calculations with respect to the penalty coefficient λ in Zhao-Parr method. In the ECDA-EXX calculations, the clusters are defined by including atoms up to the third nearest neighbors.

		$\lambda = 20$	$\lambda = 50$	$\lambda = 100$
ester	energy	-91.425	-91.416	-91.415
	dipole	1.90	1.90	1.97
	KS gap	3.41	3.36	3.40
Cl-tetracene	energy	-120.538	-120.522	-120.520
	dipole	2.37	2.38	2.38
	KS gap	1.07	0.94	0.84
tripeptide	energy	-169.201	-169.196	-169.200
	dipole	5.51	5.51	5.52
	KS gap	3.04	3.05	3.01

to the benchmarks as we increase cluster sizes. With $N_b = 3$, the errors in total energy per atom are 3 mHa, 1 mHa, and 7 mHa for ester, Cl-tetracene, and tripeptide, respectively.

We now focus on the dipole moments. Table 2 shows that, for ester and Cl-tetracene, their ECDA dipole moments with $N_b = 3$ agree well with the benchmarks. This good agreement can be explained by noting that the clusters defined with $N_b = 3$ are large enough to contain the atoms that contribute to the dipole moments. For example, the dipole moment of ester is mainly formed among O1, C1, and O2. With $N_b = 3$, the cluster of O1, the cluster of O2, and the cluster of C1 all contain O1, O2, and C1. Thus, the EXX energy density in the region of O1, C1, and O2 can be accurately patched. This well reproduces the EXX potential in that region, which in turn well reproduces the dipole moment. For Cl-tetracene, its dipole moment is mainly formed between Cl and C1. Since C1 participates in the delocalized π system of tetracene, we need to include, at least, the left-most benzene ring to define C1's cluster in order to well reproduce the EXX potential in the region of the Cl-C1 bond. With $N_b = 3$, C1's cluster contains the entire left-most benzene ring.

However, for tripeptide ECDA with $N_b = 3$ still predicts a dipole moment that is 0.51 D less than the benchmark. To explain this, we examine the dipole moment vector $\vec{D}$. With KS-DFT-EXX, we have $D_x = 5.60$ D, $D_y = -1.85$ D, $D_z = -1.24$ D. ECDA-EXX with $N_b = 3$ gives $D_x = 5.05$ D, $D_y = -1.74$ D, and $D_z = -1.35$ D. We first focus on D_y and D_z which are due to the dipole moments of the peptide bonds. ECDA-EXX gives good predictions for D_y and D_z, again due to the fact that the clusters defined with $N_b = 3$ are large enough to cover the atoms that contribute to D_y and D_z. Let's take the peptide bond O1-C1-N1-H1 for example. With $N_b = 3$, O1's cluster contains all the atoms (O1, C1, N1, and H1) belonging to this peptide bond. This is also the case for C1's cluster, N1's cluster, and H1's cluster. Therefore, the EXX potential in the region of the O1-C1-N1-H1 peptide bond is well reproduced by ECDA-EXX. As a result, the dipole moment of the peptide bond is well reproduced by ECDA-EXX. Following the similar argument, we can explain the poor agreement on D_x between ECDA-EXX and KS-DFT-EXX. D_x measures the dipole moment

along the backbone, i.e., the x direction. With $N_b = 3$, no cluster is large enough to cover the entire backbone. If the patched EXX energy in different sections of the backbone has different errors, the system's EXX potential will have different errors along the backbone. Then, ECDA-EXX will give poor prediction to D_x.

Table 2: Compare the total energies (in Hartree) and dipole moments (in Debye) from self-consistent KS-DFT-EXX and self-consistent ECDA-EXX calculations. For ECDA-EXX, the energy differences ($E_{tot}^{ECDA} - E_{tot}^{KS}$) are given with E_{tot}^{ECDA} and E_{tot}^{KS} being the total energies from KS-DFT-EXX and ECDA-EXX calculations, respectively.

	ECDA-EXX			
	$N_b = 1$	$N_b = 2$	$N_b = 3$	KS-DFT-EXX
		total energy		
ester	0.492	0.236	0.069	-91.485
Cl-tetracene	0.450	0.103	0.032	-120.555
tripeptide	0.477	0.327	0.223	-169.424
		dipole moment		
ester	1.82	1.93	1.90	1.87
Cl-tetracene	2.55	2.06	2.38	2.56
tripeptide	5.28	5.60	5.51	6.02

We also compute the energies for stretching the C1-Cl bond in Cl-tetracene using ECDA-EXX. The results are compared to the KS-DFT-EXX results (the benchmarks). Fig. 8(a) shows that ECDA-EXX energies become closer to the KS-DFT-EXX results quickly as we increase cluster sizes. The shapes of the energy curves from the two methods are similar. With $N_b = 3$, the errors per atom are less than 2 mHa for all bond lengths. By fitting the lowest three energy points on each curve with a quadratic function, the equilibrium bond lengths are 1.815 bohr, 1.731 bohr, and 1.751 bohr for ECDA-EXX calculations with $N_b = 1$, 2, and 3, respectively. They converge to the benchmark of 1.754 bohr.

The performance of ECDA-EXX is also investigated by computing the energies for removing H1, H6, and the CH_3 group from ester, as shown in Fig. 7(a). The CH_3 group is removed by cutting the bond denoted by the blue dashed line l. The energies for removing H atoms are defined as $\Delta E_{\mathrm{H}} = E_{\mathrm{rad,H}} + E_{\mathrm{H}} - E_{\mathrm{ester}}$, where $E_{\mathrm{rad,H}}$ is the energy of the H-removed radical and E_{ester} is the energy of the ester. The energy for removing the

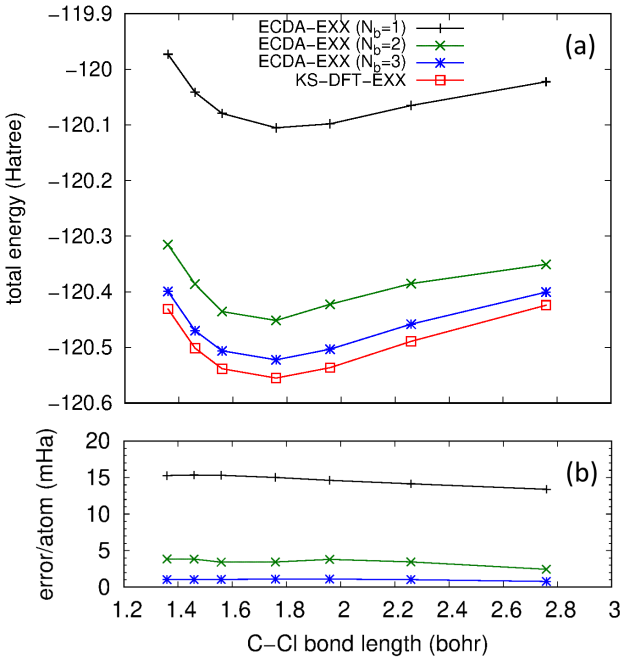

Figure 8: (a) Total energies for stretching the Cl-C1 bond of Cl-tetracene from self-consistent KS-DFT-EXX and self-consistent ECDA-EXX calculations (with N_b=1, 2, and 3). (b) Error in total energy per atom.

CH_3 group is defined as $\Delta E_{CH_3} = E_{\mathrm{rad},CH_3} + E_{CH_3} - E_{\mathrm{ester}}$, where E_{rad,CH_3} is the energy of the CH_3-removed radical. Spin-polarized ECDA-EXX calculations are performed with a smearing temperature of 0.2 eV to achieve a good convergence of the density partition in FT-DFET calculations. The penalty coefficients in the FT-DFET calculations are set to 200. The ECDA-EXX calculations are self-consistent. The benchmarks are from self-consistent KS-DFT-EXX calculations. The results are listed in Table 3. By increasing N_b, both ΔE_{H} and ΔE_{CH_3} convergence to the benchmarks; however the convergence of ΔE_{H} is much faster than that of ΔE_{CH3}. We note that the convergence of ΔE_{H} depends on the error cancellation between E_{ester} and $E_{\mathrm{rad,H}}$. For ΔE_{CH_3}, its convergence depends on the error cancellation between E_{ester} and E_{rad,CH_3}. The faster convergence observed for ΔE_{H} is then due to a better error cancellation between E_{ester} and $E_{\mathrm{rad,H}}$. This is confirmed by examining the spin densities of both H-removed and CH_3-removed radicals. The unpaired electrons in the H-removed radicals are more localized than the unpaired electron in the

CH_3-removed radical. On the other hand, the electrons of the ester molecule are well localized, because the molecule is closed shell and the electrons are all paired. Therefore, the error cancellation between E_{ester} and $E_{\text{rad,H}}$ is more effective than that between E_{ester} and $E_{\text{rad,CH}_3}$. This explains why the convergence of ΔE_{H} with N_b is faster than that of ΔE_{CH3}. To further confirm this, we also compute the energy for substituting the CH_3 group with an OH group in ester in order to avoid creating a radical. The substitution energies are defined as $E_{\text{sub}} = E_{\text{rad-OH}} + E_{\text{CH}_4} - E_{\text{ester}} - E_{\text{H}_2\text{O}}$ and are listed in Table 3. $E_{\text{rad-OH}}$ is the energy of the ester with the CH_3 group replaced by an OH group; E_{CH_4} and $E_{\text{H}_2\text{O}}$ are the energies of methane and water molecules. We expect a good error cancellation between the ECDA energies of $E_{\text{rad-OH}}$ and E_{ester}, since no unpaired electron is in these two systems. As shown in Table 3, the convergence of the substitution energy with N_b is indeed much faster than that of ΔE_{CH_3}.

Table 3: The energies for removing H1, H6, and CH_3 group in the ester molecule as illustrated in Fig. 7(a). The energy for substituting the CH_3 group with an OH group is denoted by "$CH_3 \rightarrow$ OH". Energies are in Hartree.

	ECDA-EXX				
	$N_b = 1$	$N_b = 2$	$N_b = 3$	$N_b = 4$	KS-DFT-EXX
H1	0.099	0.123	0.133	0.133	0.132
H6	0.100	0.131	0.132	0.135	0.133
CH_3	0.006	0.040	0.077	0.084	0.092
$CH_3 \rightarrow$ OH	-0.087	-0.090	-0.081	-0.078	-0.072

We also compute the energy for rotating the C3-C4 single bond in the ester as denoted in Fig. 7. The results are given in Fig. 9. The ECDA-EXX calculations are self-consistent. The benchmarks are from KS-DFT-EXX calculations. Fig. 9(a) shows that ECDA-EXX energies converge to the benchmark as N_b is increased. In Fig. 9(b), we shift the energies to make the energies of the unrotated esters to be zero. We obtain quantitative agreement on the energy profiles between ECDA-EXX and KS-DFT-EXX for $N_b \geq 4$.

For a more stringent test, we compare the EXX potentials from self-consistent KS-DFT-EXX (benchmarks) and self-consistent ECDA-EXX calculations. Fig. 10 shows the quick

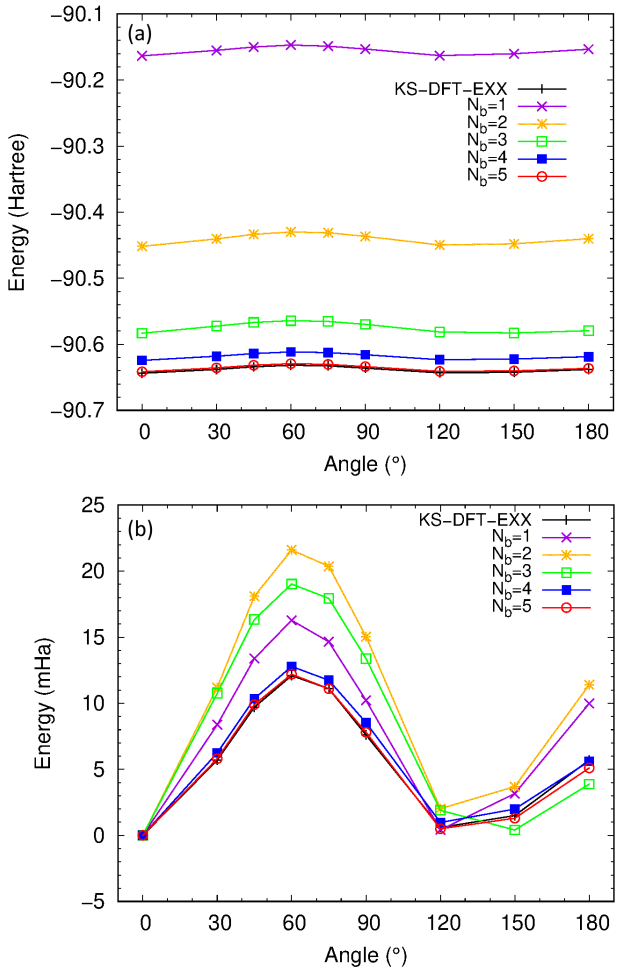

Figure 9: (a) The total energy of ester as the C3-C4 bond is rotated, from self-consistent ECDA-EXX calculations with different N_b values. The benchmarks are from self-consistent KS-DFT-EXX calculations. (b) The energies are shifted to make the total energy of the unrotated ester to zero.

convergence of ECDA's EXX potentials to the benchmark as N_b is increased. Fig. 11 compares ECDA's EXX potentials (with $N_b = 3$) to the benchmarks for the other two molecules (Cl-tetracene and tripeptide). In general, ECDA's EXX potentials agree well with the benchmarks.

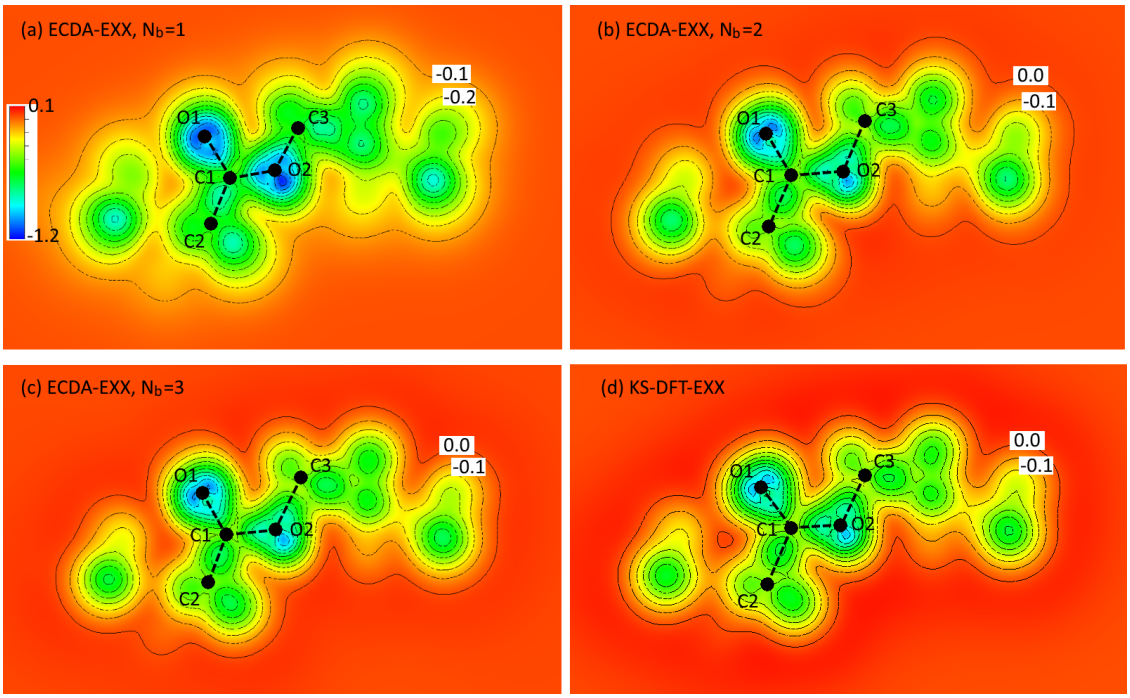

Figure 10: (a,b,c) Contour plots of ester's EXX potentials from self-consistent ECDA-EXX calculations with N_b =1, 2, and 3. (d) The EXX potential (benchmark) from self-consistent KS-DFT-EXX calculation. The atoms are labeled following Fig. 7(a). The contour planes pass through O1, C1, and O2 atoms. The interval between contour lines is 0.1 a.u. The ranges of colorbar are in atomic units.

The good agreement on EXX potentials indicates that EXX energy densities from KS-DFT-EXX calculations are well reproduced by ECDA-EXX. To verify this, we compute the atomic EXX energies according to Eq. 19, and quantify the errors by defining the absolute and relative errors

$$e_{abs,j} = E_{x,ECDA}^{atom,j} - E_{x,KS}^{atom,j} \tag{43}$$

$$e_{rel,j} = e_{abs,j}/|E_{x,KS}^{atom,j}|, \tag{44}$$

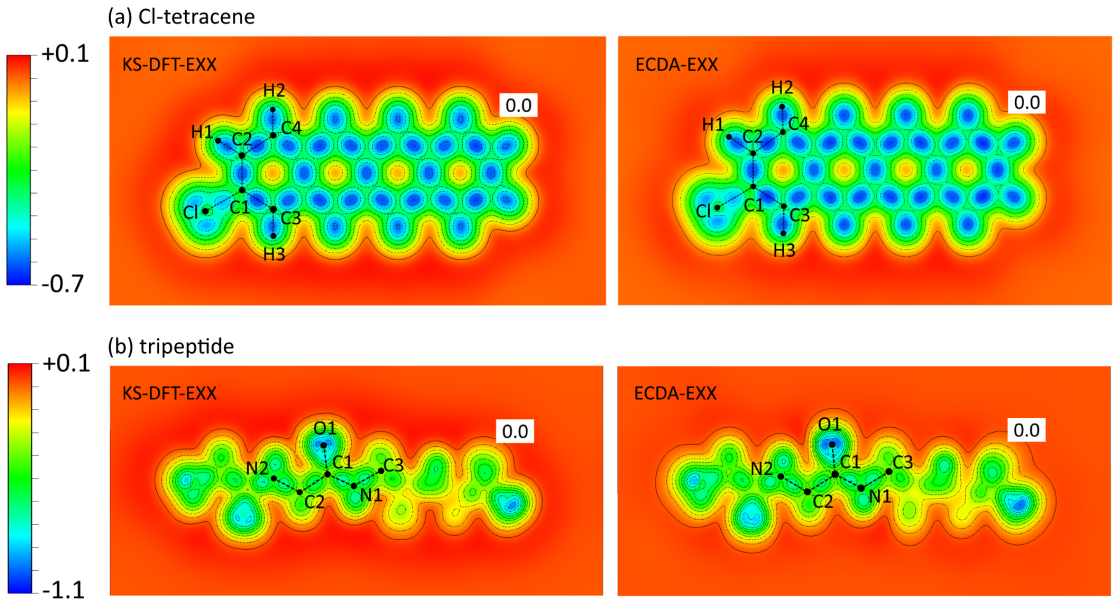

Figure 11: Contour plots of the EXX potentials of (a) Cl-tetracene and (b) tripeptide from self-consistent KS-DFT-EXX and self-consistent ECDA-EXX (with $N_b = 3$) calculations. The atoms are labeled following Fig. 7(b,c). For Cl-tetracene, the contour plane is the plane of tetracene. For tripeptide, the contour plane is defined by O1, C1, and N1 atoms. The interval between contour lines is 0.1 a.u.. The ranges of colorbars are in atomic units.

where $E_{x,ECDA}^{atom,j}$ and $E_{x,KS}^{atom,j}$ are the atomic EXX energies of the atom j from ECDA-EXX and KS-DFT-EXX calculations, respectively. The results are summarized in Fig. 12.

The upper panels of Fig. 12 (a), (b), and (c) show that in general atomic EXX energies predicted by ECDA-EXX agree well with the benchmarks. For ester, the errors on all atoms (except the two oxygen atoms) decrease quickly as we increase N_b to 3. This indicates that the exchange holes are generally delocalized over three bonds. With $N_b = 3$, $|e_{abs,j}|$ is smaller than 20 mHa and $|e_{rel,j}|$ is under 2% for all atoms. A similar observation is made for Cl-tetracene. The errors on all atoms decrease quickly as we increase N_b to 3. With $N_b = 3$, $|e_{abs,j}|$ is smaller than 10 mHa and $|e_{rel,j}|$ is under 2% for all atoms. For tripeptide, the errors do not decrease very fast as we increase N_b. The errors on some H atoms (marked by arrows) are large. Why are these H atoms special? We note that the five H atoms marked by the black arrows are bonded to the nitrogen atoms. The H atom marked by the red arrow is bonded to an oxygen atom. These marked H atoms have larger errors than the

unmarked H atoms that are bonded to the carbon atoms. Nevertheless, with $N_b = 3$, $|e_{abs,j}|$ is under 41 mHa for all atoms. $|e_{rel,j}|$ is below 2% for non-hydrogen atoms (C, N, and O) and is below 7.5% for all H atoms. To summarize, for all molecules, atomic EXX energies predicted by ECDA-EXX are close to KS-DFT-EXX results. This explains that why EXX potentials, which are the derivatives of EXX energies with respect to the electron densities, are well predicted by ECDA-EXX.

The accuracy of ECDA-EXX is further examined by comparing the system's KS eigenvalues from self-consistent ECDA-EXX and self-consistent KS-DFT-EXX (benchmarks) calculations in Fig. 13. For easy comparison, we have shifted the eigenvalues of all highest occupied molecular orbitals to zero. For ester and Cl-tetracene, the eigenvalues of the occupied states converge to the benchmarks quickly as we increase cluster sizes. For tripeptide, the convergence is slower. For the unoccupied states, the convergences of the eigenvalues are much slower for all molecules. For tripeptide, the prediction with $N_b = 3$ is even worse than the predictions from $N_b = 1$ and $N_b = 2$. This is in contrast to the case of H_{20} (Fig. 6), in which the eigenvalues of both occupied and unoccupied KS orbitals converged quickly as the clusters were made larger. The reason can be that ECDA-EXX only optimizes the systems' occupied orbitals. If we include a correlation functional (such as RPA correlation functional) that depends on both occupied and unoccupied orbitals in ECDA calculations, we expect the eigenvalues of both occupied and unoccupied KS orbitals to converge quickly to the benchmarks as we increase cluster sizes. Our expectation is based on the observation that, by adding correlation functionals to clusters, system's KS potential will also optimize clusters' correlation energies. The system's correlation energy, obtained from patching clusters' correlation energies, will then get improved as clusters are made larger, which will improve the system's unoccupied KS orbitals. We are currently implementing RPA correlation functionals for solving clusters in ABINIT and will examine this argument in a future work.

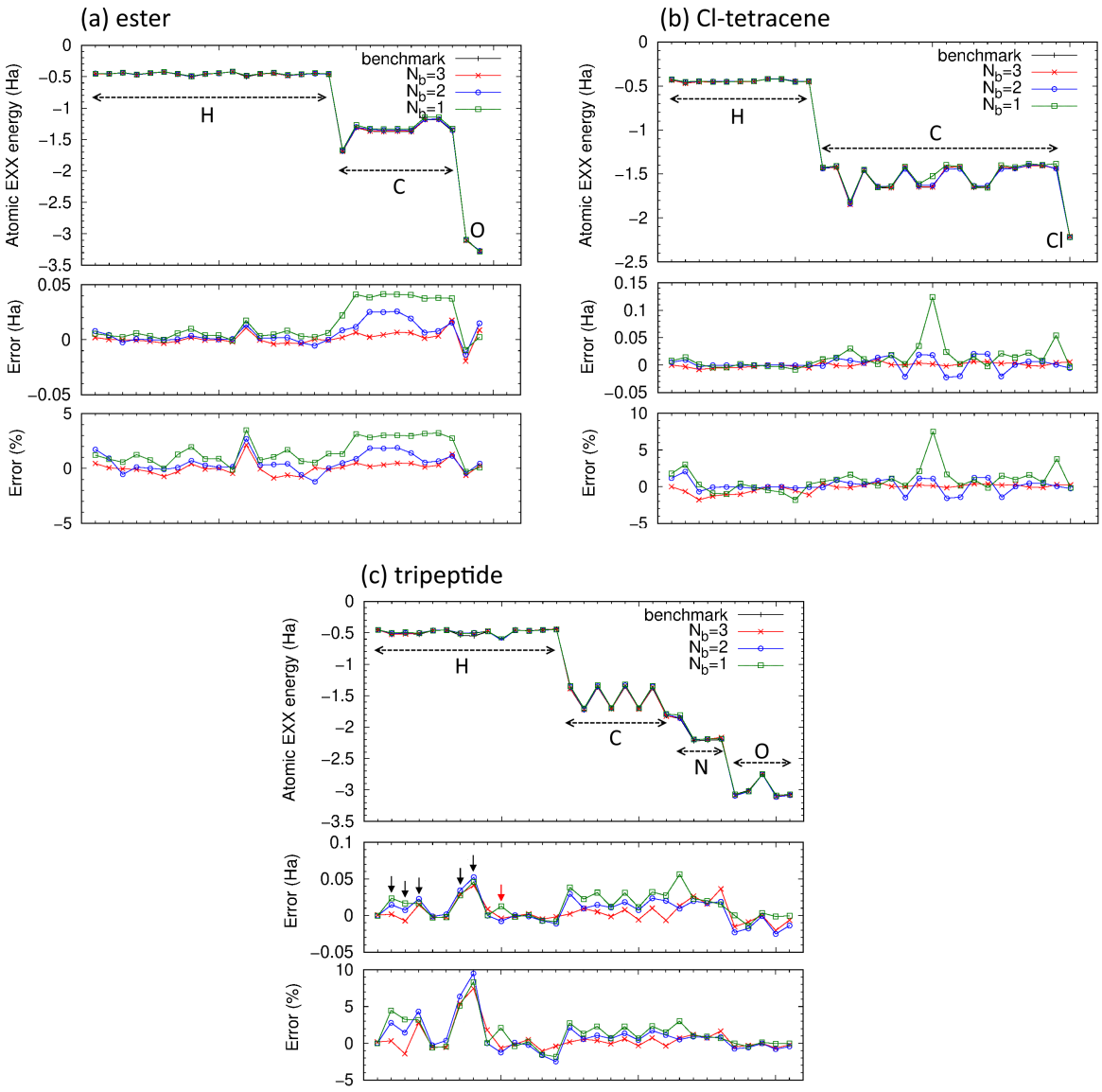

Figure 12: Atomic EXX energies of (a) ester, (b) Cl-tetracene, (c) tripeptide from self-consistent KS-DFT-EXX and self-consistent ECDA-EXX (with $N_b = 1$, 2, and 3) calculations. The x-axis denotes the atoms. For ester, the first 18 atoms are H, the next 9 atoms are C, and the last two atoms are O. For Cl-tetracene, the first 11 atoms are H, the next 18 atoms are C, and the last atom is Cl. For tripeptide, the first 14 atoms are H, the next 8 atoms are C, the following 4 atoms are N, and the last five atoms are O. The absolute and relative errors are defined in Eqs. 43 and 44.

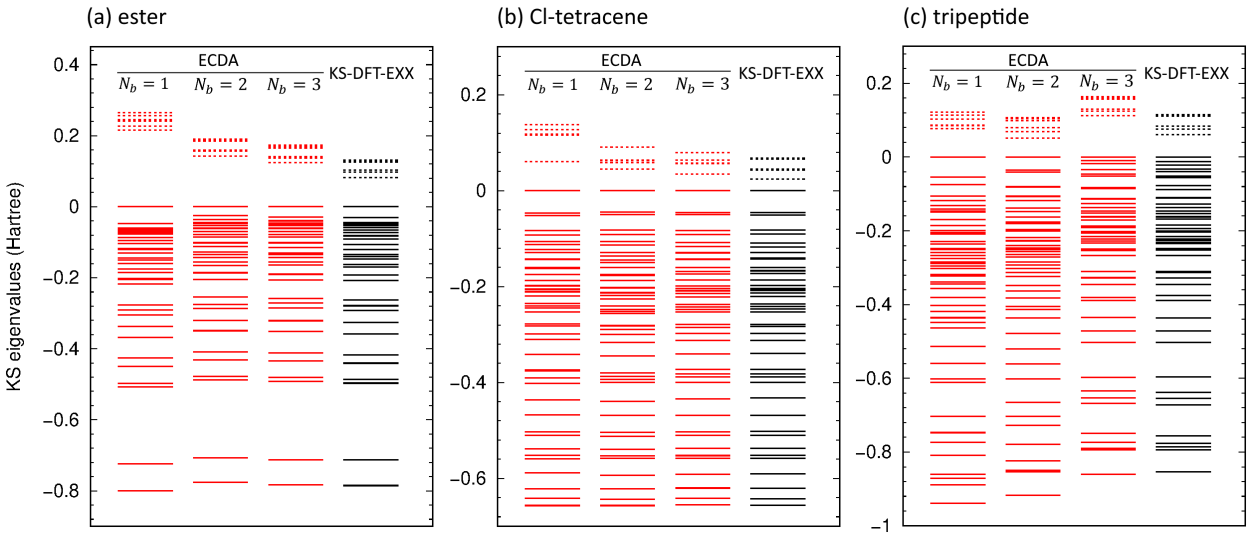

Figure 13: KS eigenvalues of (a) ester, (b) Cl-tetracene, and (c) tripeptide from self-consistent KS-DFT-EXX and self-consistent ECDA-EXX calculations. For ECDA-EXX calculations, different cluster sizes are used: $N_b = 1$, 2, and 3. The occupied and unoccupied KS orbitals are denoted by solid and dashed lines, respectively.

5 Conclusion

In this work, we developed the embedded cluster density approximation (ECDA), which is a logical extension of the local density approximation. The goal of ECDA is to scale up high-level KS-DFT simulations in large systems. In ECDA, the system's XC energy is obtained by patching high-level, locally computed XC energy densities over the system, in an atom-by-atom manner. The system's XC potential is calculated by directly taking the functional derivative of the system's XC energy with respect to the system's electron density. Since the clusters' XC energy densities depend on their embedding potentials, a numerical challenge is how to efficiently compute the the derivatives of the embedding potentials with respect to the system's KS potential. We overcome this obstacle by first deriving the relationship between the embedding potentials and the system's KS potential, and then computing all the terms that involve KS linear response functions using the first-order perturbation theory.

The computational cost of ECDA is dominated by three parts: (a) performing the Zhao-Parr method to partition the system's electron density, (b) solving Eq. 42 to compute $\{z_j\}$,

and (c) solving the OEP equation (Eq. 27) to obtain the system's XC potential. Among them, we find the Zhao-Parr method to be the most time consuming part, especially for large systems for which the environments are large. On the other hand, embedding potentials decay quickly inside the environments, and therefore we do not need to include the entire environment in the Zhao-Parr calculations. We will explore this idea in the future work to reduce the cost of Zhao-Parr method. Analytical atomic forces are necessary for efficient geometry relaxation. If clusters' electron numbers are kept fixed, ECDA is a variational method and analytical forces can be derived. We leave the discussions on the analytical forces and how well they approximate the true forces in a future work.

To examine the accuracy of ECDA, we patched EXX and RPA correlation energies in a hydrogen chain. The total energies from ECDA-RPA calculations converge quickly as we make the clusters larger. ECDA also well reproduced the system's KS eigenvalues and EXX+RPA potentials. ECDA was then applied to realistic systems: patching EXX energies in molecules. As the clusters are made larger, the total energies and dipole moments are reasonably reproduced by ECDA, and ECDA's EXX potentials converge quickly to the benchmarks. Encouraged by these promising results, we expect ECDA to be a simple, yet effective local correlation method for scaling up high-level KS-DFT calculations in large systems. This would help us resolve challenging electronic structure problems, such as, the novel electronic structures at oxides interfaces.[91]

Acknowledgement

This work is supported by the Florida State University (start-up fund) and National Science Foundation under CHE-1752769.

Supporting Information Available

The details of solving the OEP equations are given in the Supporting Information. This material is available free of charge via the Internet at http://pubs.acs.org.

Appendices

A Derivation of y_j for ACFDT EXX

We derive $y_j(\mathbf{r})$ for ACFDT EXX. A variation of the cluster's KS potential $v_{KS}^{clu,j}(\mathbf{r})$ causes change in the cluster's KS orbitals $\{\phi_k^{clu,j}\}$ and eigenvalues $\{\epsilon_k^{clu,j}\}$, where k denotes the k^{th} KS orbital. We then have

$$y_j(\mathbf{r}) = Y_{j,1}(\mathbf{r}) + Y_{j,2}(\mathbf{r}) \tag{45}$$

with

$$Y_{j,1}(\mathbf{r}) = \int d\mathbf{r}' w_j(\mathbf{r}') \sum_k \int d\mathbf{r}_2 \frac{\delta \varepsilon_{xc}^{clu,j}(\mathbf{r}')}{\delta \phi_k^{clu,j}(\mathbf{r}_2)} \frac{\delta \phi_k^{clu,j}(\mathbf{r}_2)}{\delta v_{KS}^{clu,j}(\mathbf{r})} \tag{46}$$

$$Y_{j,2}(\mathbf{r}) = \int d\mathbf{r}' w_j(\mathbf{r}') \sum_k \frac{\delta \varepsilon_{xc}^{clu,j}(\mathbf{r}')}{\delta \epsilon_k^{clu,j}} \frac{\delta \epsilon_k^{clu,j}}{\delta v_{KS}^{clu,j}(\mathbf{r})}. \tag{47}$$

For ACFDT EXX, k runs over all orbitals whose occupation numbers are not negligible. Note that the cluster's KS orbitals obtained from FD-DFET are often fractionally occupied.

Define

$$A_k^{clu,j}(\mathbf{r}_2) = \int d^3r' w_j(\mathbf{r}') \frac{\delta \varepsilon_{xc}^{clu,j}(\mathbf{r}')}{\delta \phi_k^{clu,j}(\mathbf{r}_2)}. \tag{48}$$

$Y_{j,1}(\mathbf{r})$ becomes

$$\begin{aligned} Y_{j,1}(\mathbf{r}) = & \sum_k \int d\mathbf{r}_2 A_k^{clu,j}(\mathbf{r}_2) G_k^{clu,j}(\mathbf{r}_2, \mathbf{r}) \phi_k^{clu,j}(\mathbf{r}) \\ = & \sum_k \phi_k^{clu,j}(\mathbf{r}) \psi_k^{clu,j}(\mathbf{r}). \end{aligned} \tag{49}$$

$G_k^{clu,j}(\mathbf{r}_2,\mathbf{r}) = \delta\phi_k^{clu,j}(\mathbf{r}_2)/\delta v_{KS}^{clu,j}(\mathbf{r})$ is the KS Green's function, and $\psi_k^{clu,j}(\mathbf{r})$ is the k^{th} orbital shift

$$\psi_k^{clu,j}(\mathbf{r}) = \int d\mathbf{r}_2 A_k^{clu,j}(\mathbf{r}_2) G_k^{clu,j}(\mathbf{r}_2,\mathbf{r}) \tag{50}$$

that can be efficiently calculated by solving[92,93]

$$(H_{KS} - \epsilon_k^{clu,j})\psi_k^{clu,j}(\mathbf{r}) = -(u_k^{clu,j}(\mathbf{r}) - \bar{u}_k^{clu,j})\phi_k^{clu,j}(\mathbf{r}) \tag{51}$$

where H_{KS} is the cluster's KS Hamiltonian and $u_k^{clu,j} = A_k^{clu,j}/\phi_k^{clu,j}$ and $\bar{u}_k^{clu,j} = \langle\phi_k^{clu,j}|u_k^{clu,j}|\phi_k^{clu,j}\rangle$.

It is straightforward to derive $A_k^{clu,j}$ for ACFDT EXX. For brevity, in the following we drop the superscripts that denote the cluster j.

$$\begin{aligned}
A_k(\mathbf{r}) = \quad & -\int d\mathbf{r}' w_j(\mathbf{r}') \times [\\
& \sum_{ab} f_a c_{ab} \phi_b(\mathbf{r}') \delta_{ak} \delta(\mathbf{r}' - \mathbf{r}) \int d\mathbf{r}_2 \frac{\phi_a(\mathbf{r}_2)\phi_b(\mathbf{r}_2)}{|\mathbf{r}' - \mathbf{r}_2|} + \\
& \sum_{ab} f_a c_{ab} \phi_a(\mathbf{r}') \delta_{bk} \delta(\mathbf{r}' - \mathbf{r}) \int d\mathbf{r}_2 \frac{\phi_a(\mathbf{r}_2)\phi_b(\mathbf{r}_2)}{|\mathbf{r}' - \mathbf{r}_2|} + \\
& \sum_{ab} f_a c_{ab} \phi_a(\mathbf{r}') \phi_b(\mathbf{r}') \int d\mathbf{r}_2 \frac{\delta_{ak}\delta(\mathbf{r}_2 - \mathbf{r})\phi_b(\mathbf{r}_2)}{|\mathbf{r}' - \mathbf{r}_2|} + \\
& \sum_{ab} f_a c_{ab} \phi_a(\mathbf{r}') \phi_b(\mathbf{r}') \int d\mathbf{r}_2 \frac{\delta_{bk}\delta(\mathbf{r}_2 - \mathbf{r})\phi_a(\mathbf{r}_2)}{|\mathbf{r}' - \mathbf{r}_2|}]
\end{aligned} \tag{52}$$

where a and b run over all the orbitals that have non-negligible occupation numbers. We only consider the non-spin polarized case. ϕ_a and f_a are the a^{th} KS orbital and its occupation number of the cluster j, and $c_{ab} = 1 + \mathrm{sgn}(\epsilon_a^{clu,j} - \epsilon_b^{clu,j})$. Above expression can be simplified to

$$A_k(\mathbf{r}) = -\sum_b (f_k c_{kb} + f_b c_{bk}) \phi_b(\mathbf{r}) \int d\mathbf{r}_2 (w_j(\mathbf{r}) + w_j(\mathbf{r}_2)) \frac{\phi_k(\mathbf{r}_2)\phi_b(\mathbf{r}_2)}{|\mathbf{r} - \mathbf{r}_2|}. \tag{53}$$

The calculation of $Y_{j,2}(\mathbf{r})$ is straightforward, since EXX energy density explicitly depends on the occupation numbers which in turn depend on KS eigenvalues. In addition, we have

$\delta\epsilon_k^{clu,j}/\delta v_{KS}^{clu,j}(\mathbf{r}) = \phi_k^{clu,j}(\mathbf{r})\phi_k^{clu,j}(\mathbf{r})$ due to the first-order perturbation theory.

References

(1) Hohenberg, P.; Kohn, W. Inhomogeneous electron gas. *Phys. Rev.* **1964**, *136*, B864.

(2) Kohn, W.; Sham, L. J. Self-consistent equations including exchange and correlation effects. *Phys. Rev.* **1965**, *140*, A1133.

(3) Perdew, J. P.; Schmidt, K. Jacob's ladder of density functional approximations for the exchange-correlation energy. AIP Conf. Proc. 2001; pp 1–20.

(4) Harris, J.; Jones, R. O. The surface energy of a bounded electron gas. *J. Phys. F: Met. Phys.* **1974**, *4*, 1170–1186.

(5) Langreth, D. C.; Perdew, J. P. The exchange-correlation energy of a metallic surface. *Solid State Commun.* **1975**, *17*, 1425–1429.

(6) Gunnarsson, O.; Lundqvist, B. I. Exchange and correlation in atoms, molecules, and solids by the spin-density-functional formalism. *Phys. Rev. B* **1976**, *13*, 4274.

(7) Langreth, D. C.; Perdew, J. P. Exchange-correlation energy of a metallic surface wave-vector analysis. *Phys. Rev. B* **1977**, *15*, 2884.

(8) Dobson, J. F.; Wang, J. Successful Test of a Seamless van der Waals Density Functional. *Phys. Rev. Lett.* **1999**, *82*, 2123–2126.

(9) Lein, M.; Dobson, J. F.; Gross, E. K. U. Toward the description of van der Waals interactions within density functional theory. *J. Comput. Chem.* **1999**, *20*, 12–22.

(10) Furche, F. Molecular tests of the random phase approximation to the exchange-correlation energy functional. *Phys. Rev. B* **2001**, *64*, 195120.

(11) Fuchs, M.; Gonze, X. Accurate density functionals: Approaches using the adiabatic-connection fluctuation-dissipation theorem. *Phys. Rev. B* **2002**, *65*, 235109.

(12) Heßelmann, A.; Görling, A. Random phase approximation correlation energies with exact Kohn–Sham exchange. *Mol. Phys.* **2010**, *108*, 359–372.

(13) Grabowski, I.; Hirata, S.; Ivanov, S.; Bartlett, R. J. Ab initio density functional theory: OEP-MBPT(2). A new orbital-dependent correlation functional. *J. Chem. Phys.* **2002**, *116*, 4415–4425.

(14) Bartlett, R. J.; Grabowski, I.; Hirata, S.; Ivanov, S. The exchange-correlation potential inab initiodensity functional theory. *J. Chem. Phys.* **2005**, *122*, 034104.

(15) Erhard, J.; Bleiziffer, P.; Görling, A. Power Series Approximation for the Correlation Kernel Leading to Kohn-Sham Methods Combining Accuracy, Computational Efficiency, and General Applicability. *Phys. Rev. Lett.* **2016**, *117*, 143002.

(16) Kohn, W. Density Functional and Density Matrix Method Scaling Linearly with the Number of Atoms. *Phys. Rev. Lett.* **1996**, *76*, 3168–3171.

(17) Prodan, E.; Kohn, W. Nearsightedness of electronic matter. *Proc. Natl. Acad. Sci. U. S. A.* **2005**, *102*, 11635–11638.

(18) Prodan, E. Nearsightedness of electronic matter in one dimension. *Phys. Rev. B* **2006**, *73*, 085108.

(19) Pulay, P. Localizability of dynamic electron correlation. *Chem. Phys. Lett.* **1983**, *100*, 151–154.

(20) Saebo, S.; Pulay, P. Local configuration interaction: An efficient approach for larger molecules. *Chem. Phys. Lett.* **1985**, *113*, 13–18.

(21) Kirtman, B.; Dykstra, C. E. Local space approximation for configuration interaction and coupled cluster wave functions. *J. Chem. Phys.* **1986**, *85*, 2791–2796.

(22) Stoll, H. Correlation energy of diamond. *Phys. Rev. B* **1992**, *46*, 6700–6704.

(23) Knizia, G.; Chan, G. K.-L. Density matrix embedding: A simple alternative to dynamical mean-field theory. *Phys. Rev. Lett.* **2012**, *109*, 186404.

(24) Yang, W. Direct calculation of electron density in density-functional theory. *Phys. Rev. Lett.* **1991**, *66*, 1438.

(25) Wang, L.-W. Charge-Density Patching Method for Unconventional Semiconductor Binary Systems. *Phys. Rev. Lett.* **2002**, *88*, 256402.

(26) Kohn, W.; Mattsson, A. E. Edge electron gas. *Phys. Rev. Lett.* **1998**, *81*, 3487.

(27) Armiento, R.; Mattsson, A. E. Subsystem functionals in density-functional theory: Investigating the exchange energy per particle. *Phys. Rev. B* **2002**, *66*, 165117.

(28) Armiento, R.; Mattsson, A. E. Functional designed to include surface effects in self-consistent density functional theory. *Phys. Rev. B* **2005**, *72*, 085108.

(29) Zhu, T.; de Silva, P.; van Aggelen, H.; Van Voorhis, T. Many-electron expansion: A density functional hierarchy for strongly correlated systems. *Phys. Rev. B* **2016**, *93*, 201108.

(30) Knizia, G.; Chan, G. K.-L. Density matrix embedding: A strong-coupling quantum embedding theory. *J. Chem. Theory Comput.* **2013**, *9*, 1428–1432.

(31) Blöchl, P. E.; Walther, C. F. J.; Pruschke, T. Method to include explicit correlations into density-functional calculations based on density-matrix functional theory. *Phys. Rev. B* **2011**, *84*, 205101.

(32) Wu, X.; Selloni, A.; Car, R. Order-N implementation of exact exchange in extended insulating systems. *Phys. Rev. B* **2009**, *79*, 085102.

(33) Kállay, M. Linear-scaling implementation of the direct random-phase approximation. *J. Chem. Phys.* **2015**, *142*, 204105.

(34) Schurkus, H. F.; Ochsenfeld, C. Communication: An effective linear-scaling atomic-orbital reformulation of the random-phase approximation using a contracted double-Laplace transformation. *J. Chem. Phys.* **2016**, *144*, 031101.

(35) Luenser, A.; Schurkus, H. F.; Ochsenfeld, C. Vanishing-Overhead Linear-Scaling Random Phase Approximation by Cholesky Decomposition and an Attenuated Coulomb-Metric. *J. Chem. Theory Comput.* **2017**, *13*, 1647–1655.

(36) Senatore, G.; Subbaswamy, K. Density dependence of the dielectric constant of rare-gas crystals. *Phys. Rev. B* **1986**, *34*, 5754.

(37) Cortona, P. Self-consistently determined properties of solids without band-structure calculations. *Phys. Rev. B* **1991**, *44*, 8454.

(38) Wesolowski, T. A.; Warshel, A. Frozen density functional approach for ab initio calculations of solvated molecules. *J. Phys. Chem.* **1993**, *97*, 8050–8053.

(39) Govind, N.; Wang, Y.; Da Silva, A.; Carter, E. Accurate ab initio energetics of extended systems via explicit correlation embedded in a density functional environment. *Chem. Phys. Lett.* **1998**, *295*, 129–134.

(40) Neugebauer, J.; Louwerse, M. J.; Baerends, E. J.; Wesolowski, T. A. The merits of the frozen-density embedding scheme to model solvatochromic shifts. *J. Chem. Phys.* **2005**, *122*, 094115.

(41) Jacob, C. R.; Visscher, L. Calculation of nuclear magnetic resonance shieldings using frozen-density embedding. *J. Chem. Phys.* **2006**, *125*, 194104.

(42) Cohen, M. H.; Wasserman, A. On hardness and electronegativity equalization in chemical reactivity theory. *J. Chem. Phys.* **2006**, *125*, 1121–1139.

(43) Roncero, O.; de Lara-Castells, M. P.; Villarreal, P.; Flores, F.; Ortega, J.; Paniagua, M.; Aguado, A. An inversion technique for the calculation of embedding potentials. *J. Chem. Phys.* **2008**, *129*, 184104.

(44) Goodpaster, J. D.; Ananth, N.; Manby, F. R.; Miller, T. F. Exact nonadditive kinetic potentials for embedded density functional theory. *J. Chem. Phys.* **2010**, *133*, 084103.

(45) Huang, C.; Pavone, M.; Carter, E. A. Quantum mechanical embedding theory based on a unique embedding potential. *J. Chem. Phys.* **2011**, *134*, 154110.

(46) Laricchia, S.; Fabiano, E.; Della Sala, F. Frozen density embedding with hybrid functionals. *J. Chem. Phys.* **2010**, *133*, 164111.

(47) Fux, S.; Jacob, C. R.; Neugebauer, J.; Visscher, L.; Reiher, M. Accurate frozen-density embedding potentials as a first step towards a subsystem description of covalent bonds. *J. Chem. Phys.* **2010**, *132*, 164101.

(48) Pavanello, M.; Neugebauer, J. Modelling charge transfer reactions with the frozen density embedding formalism. *J. Chem. Phys.* **2011**, *135*, 234103.

(49) Jacob, C. R.; Neugebauer, J. Subsystem density-functional theory. *Wiley Interdiscip. Rev.: Comput. Mol. Sci.* **2014**, *4*, 325–362.

(50) Novák, P.; Kuneš, J.; Chaput, L.; Pickett, W. Exact exchange for correlated electrons. *Phys. Status Solidi B* **2006**, *243*, 563–572.

(51) Manby, F. R.; Stella, M.; Goodpaster, J. D.; Miller III, T. F. A simple, exact density-functional-theory embedding scheme. *J. Chem. Theory Comput.* **2012**, *8*, 2564–2568.

(52) Fornace, M. E.; Lee, J.; Miyamoto, K.; Manby, F. R.; Miller III, T. F. Embedded Mean-Field Theory. *J. Chem. Theory Comput.* **2015**, *11*, 568–580.

(53) Pernal, K. Reduced density matrix embedding: General formalism and inter-domain correlation functional. *Phys. Chem. Chem. Phys.* **2016**, *18*, 21111–21121.

(54) Huang, C. Patching the Exchange-Correlation Potential in Density Functional Theory. *J. Chem. Theory Comput.* **2016**, *12*, 2224–2233.

(55) Huang, C. Extending the density functional embedding theory to finite temperature and an efficient iterative method for solving for embedding potentials. *J. Chem. Phys.* **2016**, *144*, 124106.

(56) Becke, A. D. A multicenter numerical integration scheme for polyatomic molecules. *J. Chem. Phys.* **1988**, *88*, 2547–2553.

(57) Zhao, Q.; Parr, R. G. Quantities Ts[n] and Tc[n] in density-functional theory. *Phys. Rev. A* **1992**, *46*, 2337.

(58) Zhao, Q.; Parr, R. G. Constrained-search method to determine electronic wave functions from electronic densities. *J. Chem. Phys.* **1993**, *98*, 543–548.

(59) Zhao, Q.; Morrison, R. C.; Parr, R. G. From electron densities to Kohn-Sham kinetic energies, orbital energies, exchange-correlation potentials, and exchange-correlation energies. *Phys. Rev. A* **1994**, *50*, 2138.

(60) Kerker, G. Efficient iteration scheme for self-consistent pseudopotential calculations. *Phys. Rev. B* **1981**, *23*, 3082.

(61) Harl, J.; Schimka, L.; Kresse, G. Assessing the quality of the random phase approximation for lattice constants and atomization energies of solids. *Phys. Rev. B* **2010**, *81*, 115126.

(62) Perdew, J. P.; Ruzsinszky, A.; Csonka, G. I.; Vydrov, O. A.; Scuseria, G. E.; Staroverov, V. N.; Tao, J. Exchange and correlation in open systems of fluctuating electron number. *Phys. Rev. A* **2007**, *76*, 040501.

(63) Yan, Z.; Perdew, J. P.; Kurth, S. Density functional for short-range correlation: Accuracy of the random-phase approximation for isoelectronic energy changes. *Phys. Rev. B* **2000**, *61*, 16430.

(64) Sharp, R.; Horton, G. A variational approach to the unipotential many-electron problem. *Phys. Rev.* **1953**, *90*, 317.

(65) Talman, J. D.; Shadwick, W. F. Optimized effective atomic central potential. *Phys. Rev. A* **1976**, *14*, 36.

(66) Sahni, V.; Gruenebaum, J.; Perdew, J. Study of the density-gradient expansion for the exchange energy. *Phys. Rev. B* **1982**, *26*, 4371.

(67) Kümmel, S.; Kronik, L. Orbital-dependent density functionals: Theory and applications. *Rev. Mod. Phys.* **2008**, *80*, 3.

(68) de Gironcoli, S. Lattice dynamics of metals from density-functional perturbation theory. *Phys. Rev. B* **1995**, *51*, 6773–6776.

(69) Pulay, P. Convergence acceleration of iterative sequences. the case of scf iteration. *Chem. Phys. Lett.* **1980**, *73*, 393–398.

(70) Schipper, P. R. T.; Gritsenko, O. V.; Baerends, E. J. One-determinantal pure state versus ensemble Kohn-Sham solutions in the case of strong electron correlation: CH2 and C2. *Theor. Chem. Acc.* **1998**, *99*, 329–343.

(71) Ullrich, C.; Kohn, W. Kohn-Sham theory for ground-state ensembles. *Phys. Rev. Lett.* **2001**, *87*, 093001.

(72) Morrison, R. C. Electron correlation and noninteracting v-representability in density functional theory: The Be isoelectronic series. *J. Chem. Phys.* **2002**, *117*, 10506–10511.

(73) Katriel, J.; Roy, S.; Springborg, M. A study of the adiabatic connection for two-electron systems. *J. Chem. Phys.* **2004**, *121*, 12179–12190.

(74) van Leeuwen, R. Density functional approach to the many-body problem: key concepts and exact functionals. *Adv. Quantum Chem.* **2003**, *43*, 25–94.

(75) Chayes, J. T.; Chayes, L.; Ruskai, M. B. Density functional approach to quantum lattice systems. *J. Stat. Phys.* **1985**, *38*, 497–518.

(76) Dandrea, R. G.; Ashcroft, N. W.; Carlsson, A. E. Electron liquid at any degeneracy. *Phys. Rev. B* **1986**, *34*, 2097–2111.

(77) Eschrig, H. T>0 ensemble-state density functional theory via Legendre transform. *Phys. Rev. B* **2010**, *82*, 205120.

(78) Pittalis, S.; Proetto, C. R.; Floris, A.; Sanna, A.; Bersier, C.; Burke, K.; Gross, E. K. U. Exact Conditions in Finite-Temperature Density-Functional Theory. *Phys. Rev. Lett.* **2011**, *107*, 163001.

(79) *MATLAB (Version 2015a), The MathWorks Inc., Natick, MA, USA*

(80) Huang, C.; Chi, Y.-C. Directly patching high-level exchange-correlation potential based on fully determined optimized effective potentials. *J. Chem. Phys.* **2017**, *147*, 244111.

(81) Wagner, L. O.; Stoudenmire, E.; Burke, K.; White, S. R. Reference electronic structure calculations in one dimension. *Phys. Chem. Chem. Phys.* **2012**, *14*, 8581–8590.

(82) Helbig, N.; Fuks, J. I.; Casula, M.; Verstraete, M. J.; Marques, M.; Tokatly, I.; Rubio, A. Density functional theory beyond the linear regime: Validating an adiabatic local density approximation. *Phys. Rev. A* **2011**, *83*, 032503.

(83) Wu, Q.; Yang, W. A direct optimization method for calculating density functionals and exchange–correlation potentials from electron densities. *J. Chem. Phys.* **2003**, *118*, 2498–2509.

(84) Gonze, X. et al. ABINIT: First-principles approach to material and nanosystem properties. *Comput. Phys. Commun.* **2009**, *180*, 2582–2615.

(85) Perdew, J. P.; Burke, K.; Ernzerhof, M. Generalized gradient approximation made simple. *Phys. Rev. Lett.* **1996**, *77*, 3865.

(86) Genovese, L.; Deutsch, T.; Neelov, A.; Goedecker, S.; Beylkin, G. Efficient solution of Poisson's equation with free boundary conditions. *J. Chem. Phys.* **2006**, *125*, 074105.

(87) Genovese, L.; Deutsch, T.; Goedecker, S. Efficient and accurate three-dimensional Poisson solver for surface problems. *J. Chem. Phys.* **2007**, *127*, 054704.

(88) Paier, J.; Marsman, M.; Hummer, K.; Kresse, G.; Gerber, I. C.; Ángyán, J. G. Screened hybrid density functionals applied to solids. *J. Chem. Phys.* **2006**, *124*, 154709.

(89) Momma, K.; Izumi, F. VESTA3 for three-dimensional visualization of crystal, volumetric and morphology data. *J. Appl. Crystallogr.* **2011**, *44*, 1272–1276.

(90) Akama, T.; Fujii, A.; Kobayashi, M.; Nakai, H. Is the divide-and-conquer Hartree–Fock method valid for calculations of delocalized systems? *Mol. Phys.* **2007**, *105*, 2799–2804.

(91) Ohtomo, A.; Hwang, H. A high-mobility electron gas at the LaAlO3/SrTiO3 heterointerface. *Nature* **2004**, *427*, 423–426.

(92) Krieger, J.; Li, Y.; Iafrate, G. Construction and application of an accurate local spin-polarized Kohn-Sham potential with integer discontinuity: Exchange-only theory. *Phys. Rev. A* **1992**, *45*, 101.

(93) Kümmel, S.; Perdew, J. P. Simple Iterative Construction of the Optimized Effective Potential for Orbital Functionals, Including Exact Exchange. *Phys. Rev. Lett.* **2003**, *90*, 043004.

Graphical TOC Entry